ELSEVIER

Quaternary Science Reviews 26 (2007) 1818–1837

QSR

Simulating the transient evolution and abrupt change of Northern Africa atmosphere–ocean–terrestrial ecosystem in the Holocene ☆

Z. Liu[a,*], Y. Wang[a], R. Gallimore[a], F. Gasse[b], T. Johnson[c], P. deMenocal[d], J. Adkins[e], M. Notaro[a], I.C. Prentice[f], J. Kutzbach[a], R. Jacob[g], P. Behling[a], L. Wang[a], E. Ong[a]

[a]*Center for Climatic Research, University of Wisconsin-Madison, CCR, 1225 W. Dayton St., Madison, WI 53706, USA*
[b]*CEREGE, BP 80, 13545, Aix-en-Provence, cedex 04, France*
[c]*Large Lakes Observatory, Department of Geological Sciences, University of Minnesota-Duluth, MN, USA*
[d]*Lamont-Doherty Earth Observatory of Columbia University, USA*
[e]*California Institute of Technology, CA, USA*
[f]*Department of Earth Sciences, University of Bristol, UK*
[g]*Argonne National Laboratory, DOE, USA*

Received 30 July 2006; received in revised form 22 February 2007; accepted 1 March 2007

Abstract

We present the first synchronously coupled transient simulation of the evolution of the northern Africa climate-ecosystem for the last 6500 years in a global general circulation ocean–atmosphere–terrestrial ecosystem model. The model simulated the major abrupt vegetation collapse in the southern Sahara at about 5 ka, consistent with the proxy records. Local precipitation, however, shows a much more gradual decline with time, implying a lack of strong positive vegetation feedback on annual rainfall during the collapse. The vegetation change in northern Africa is driven by local precipitation decline and strong precipitation variability. In contrast, the change of precipitation is dominated by internal climate variability and a gradual monsoonal climate response to orbital forcing. In addition, some minor vegetation changes are also simulated in different regions across northern Africa

The model also simulated a gradual annual mean surface cooling in the subtropical North Atlantic towards the latest Holocene, as well as a reduced seasonal cycle of SST. The SST response is caused largely by the insolation forcing, while the annual mean cooling is also reinforced by the increased coastal upwelling near the east boundary. The increased upwelling results from a southward retreat of the North Africa monsoon system, and, in turn, an increased northeasterly trade wind. The simulated changes of SST and upwelling are also largely consistent with marine proxy records, albeit with a weaker magnitude in the model.

The mismatch between the collapse of vegetation and gradual transition of rainfall suggests that the vegetation collapse is not caused by a strong positive vegetation feedback. Instead, it is suggested that the Mid-Holocene collapse of North African vegetation is caused mainly by a nonlinear response of the vegetation to a precipitation threshold in the presence of strong climate variability. The implication to the modeling and observations is also discussed.

1. Introduction

One of the most important environmental changes in the last 10,000 years is the abrupt desertification of northern Africa Relative to the Early and Mid-Holocene, present North Africa is much drier, with greatly expanded deserts, and greatly reduced vegetation cover (Hoelzmann et al., 1998; Jolly et al., 1998) and lake areas (Gasse et al., 1990; Gasse and Van Campo, 1994; Gasse, 2000, 2002) (Fig. 1). Previous modeling studies suggest that this Africa aridification is caused by a reduction of summer insolation, and in turn, the North African summer monsoon towards the present (Kutzbach and Otto-Bliesner, 1982; Kutzbach and Street-Perrott, 1985); the insolation effect could be further enhanced by positive feedbacks from the vegetation (Kutzbach et al., 1996; Claussen and Gayler, 1997) through surface albedo (Charney, 1975; Kitoh et al., 1988) and evapotranspiration and soil moisture (Shukla and Mintz,

☆CCR contribution number: 911.

*Corresponding author. Tel.: +1 608 262 0777.
E-mail address: zliu3@wisc.edu (Z. Liu).

0277-3791/$ - see front matter © 2007 Elsevier Ltd. All rights reserved.
doi:10.1016/j.quascirev.2007.03.002

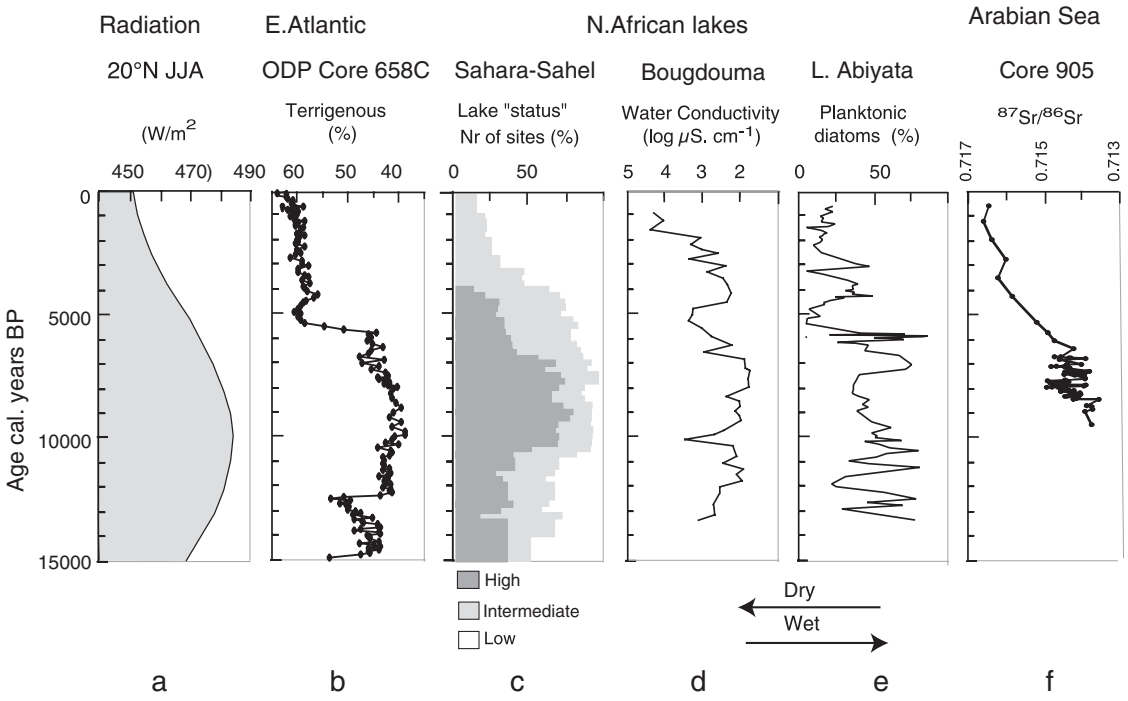

Fig. 1. Comparison of marine off, and lake records of North Africa, compared with solar radiation. (a) Summer insolation at 20°N (Berger and Loutre, 1991). (b) Dust record off northwestern Africa (deMenocal et al., 2000); (c–e) Lacustrine indicators of the precipitation–evaporation balance (See later Fig. 7 for site location); (c) summary of lake-level fluctuations in the Sahara–Sahel belt, 8–28°N, 20°W–40°E (after Hoelzmann, et al., 1998, 2004); (d) Lake water diatom-inferred conductivity at Bougdouma (Niger, 13°20′N, 11°40′E; Gasse, 2002); (e) Planktonic diatom percentages at Lake Abiyata (Ethiopia, 7°40′N–38°40′E; Chalié and Gasse, 2002); (f) dust-borne radiogenic isotope record off Somalia (Core 905P; Jung et al., 2004).

1982; Xue and Shukla, 1993); it can also be enhanced by a positive feedback from the nearby ocean (Kutzbach and Liu, 1997).

One distinct feature of the reconstructed Africa desertification in the Mid-Holocene is its abruptness, relative to the gradual insolation. The overall lake-level fluctuation in the Sahara–Sahel belt, albeit with a coarse temporal resolution, indicates a relatively faster decline between 6000 and 4000 years ago (6–4 ka) (Hoelzmann et al., 1998, 2004; Fig. 1c), relative to the gradual insolation forcing (Fig. 1a). Some recent high-resolution records appear to suggest an abrupt termination of the African Humid Period within a century in the Mid-Holocene, most notably shown in an abrupt increase of terrigenous dust deposition in the tropical Atlantic sediment (Fig. 1b) (deMenocal et al., 2000; Adkins et al., 2006) and an abrupt decrease of planktonic diatoms at Lake Abiyata in Ethiopia (Fig. 1e; Chalié and Gasse, 2002). In addition to this dominant abrupt change in the Mid-Holocene, there are also indications of a variety of regional climate-ecosystem evolutions in northern Africa For example, a more complex and more gradual change after 4.5 ka is seen in the diatom-inferred lake water conductivity at Bougdouma (Niger, Fig. 1d; Gasse, 2002) and the dust-borne sediment records off Somalia (Jung et al., 2004; Fig. 1f). Lake Turkana at 4°N in the East African Rift Valley, experienced an abrupt rise in salinity according to the diatom record, presumably associated with a significant drop in lake level, at about 4.3 ka (Halfman et al., 1992). Lake Edward, situated on the equator in the western arm of the Rift Valley, experienced the onset of Mid-Holocene aridity around 5.2 ka, when endogenic calcite first appears in the sediment record (Russell et al., 2003). Lake Victoria, just 250 km to the east of Lake Edward, displays no evidence for increased aridity in the Mid-Holocene (Johnson et al., 2000) and Lake Malawi, at 10–14 °S, experienced a shift to wetter conditions in the Mid-Holocene, consistent with enhanced summer insolation in the Southern Hemisphere at that time (Finney and Johnson, 1991). Given the same gradual change of the insolation forcing (Fig. 1a), it is important to understand why the desertification occurred so abruptly in northern Africa It is also interesting to explore why there are regional differences in the evolution of climate-ecosystem.

Recent interest in the abrupt Africa aridification in the Holocene was also motivated by a series of modeling studies that show possible multiple equilibriums in the climate–terrestrial ecosystem over the northern Africa In these studies, a comprehensive (general circulation) atmosphere model was coupled to a terrestrial biome model iteratively between their equilibrium responses.[1] Strong positive vegetation feedback and multiple solutions were

[1]This so-called equilibrium asynchronous coupling scheme, under certain conditions, can be shown as a crude scheme for the simulation of long-term feedbacks in a coupled system (Liu et al., 1999).

found in the West Africa for the present-day (Claussen, 1994, 1997, 1998) and Last Glacial Maximum (Kubatzki and Claussen, 1998), while a single equilibrium was found for the Mid-Holocene (Claussen and Gayler, 1997). Later, similar positive vegetation feedback and multiple equilibriums were also found in synchronously coupled models of intermediate complexity (e.g. Wang and Eltahir, 2000; Zeng and Neelin, 2000). These studies gave the impression of a robust multiple equilibrium solutions in the northern Africa climate–biome system. In the theory of dynamic systems, this multiple equilibria would imply a possible abrupt change of the coupled system under a gradual forcing. That is, the abrupt change can be caused by a strong positive vegetation–climate feedback, which leads to multiple equilibrium states, and, in turn a sudden collapse from a green Sahara state to a desert state under a gradually decreasing summer insolation. By examining the stability property in their coupled models, Claussen et al. (1998) and Brovkin et al. (1998) predicted an abrupt change of northern Africa climate-ecosystem approximately in between 6000 and 4000 yr BP.

These studies on the abrupt change of Africa climate-ecosystem further motivated a series of transient Holocene simulations that attempt to simulate the abrupt change explicitly, mostly in coupled models of intermediate complexity. Claussen et al. (1999) (hereafter C99) were the first to simulate an abrupt (relative to the orbital forcing) change in Africa climate-ecosystem in the Mid-Holocene, which was later "validated" by the dust record of deMenocal et al. (2000). The abrupt change in C99 is associated with a strong positive vegetation feedback on climate, but does not seem to be induced by an unstable bifurcation of the coupled system—a point to be returned later. This abrupt collapse in the Mid-Holocene, however, was not simulated in follow-up studies which all used the same vegetation model as C99. Coupled with a quasi-geostrophic atmosphere model that has strong internal variability, Renssen et al. (2003) simulated a Holocene climate evolution that exhibits too frequent and strong swings between the green/humid and desert/dry periods, but without dominant abrupt collapse events; this result is suggested to be related to their model multiple equilibriums in the Mid-Holocene and a single equilibrium at the present. Coupled with different energy balance atmosphere models, respectively, Brovkin et al. (2002) and Wang et al. (2005) only generate a gradual decline in their climate–vegetation systems. The strong model-dependence of the simulation of the abrupt change in these intermediate models suggest a complex nature of the abrupt change.

Coupled general circulation models (GCM) are the most comprehensive models for climate study. Due to the computational limitation, however, coupled GCM simulations have been used mostly for "snapshot" experiments, with each snapshot for hundreds of years forced by a fixed climate forcing (e.g. Liu et al., 2003a, b; Hewitt and Mitchell, 1998). The snapshot experiment is useful for the study of the equilibrium climate response and the inference of long-term climate trend, but is deficient for addressing the nature of the transient evolution and abrupt change. Most recently, Schurgers et al. (2006) used a comprehensive coupled GCM to simulate the evolution of the climate-ecosystem during the Holocene. However, their atmosphere model is coupled *asynchronously* with the ocean and biome models. The asynchronous coupling scheme is perhaps valid for the simulation of long-term climate trends, but it not proper for the study of abrupt change, because of the distortion on short-term coupled climate variability and in turn abrupt change. Nevertheless, the Holocene simulation of Schurgers et al. (2006) exhibits a strong variability with no major collapse in the Mid-Holocene, somewhat similar to Renssen et al. (2003), providing another example of unsuccessful simulation of the abrupt change.

Here, we present the first transient simulation of the global climate-terrestrial ecosystem of the last 6500 years in a *synchronously* coupled *general circulation* atmosphere–ocean-dynamic vegetation model—FOAM-LPJ (Fast Ocean Atmosphere Model—Lund-Potsdam-Jena). Our objective is to understand the nature of the transient evolution, especially the abrupt change, of the climate-ecosystem in northern Africa in light of the combined marine and terrestrial proxy paleoclimate records. The higher spatial resolution of our model, relative to previous models of intermediate complexity, allows us to simulate a variety of climate-ecosystem evolution behaviors over northern Africa The dominant vegetation change occurs as an abrupt collapse at about 5 ka, consistent with proxy records (deMenocal et al., 2000). The local rainfall, however, exhibits a much less abrupt change accompanying the vegetation collapse. In addition, our model simulation produces a gradual annual mean surface cooling and an enhanced upwelling towards the latest Holocene in the coastal North Atlantic, consistent with marine proxy analyses (Zhao et al., 1995; Bard et al., 2000; Pailler and Bard, 2002; Adkins et al., 2006). The cooling results from both the reduced insolation forcing in summer as well as the enhanced coastal upwelling throughout the year. The abrupt vegetation change, and the relatively gradual change of precipitation and climate, prompted the hypothesis that the abrupt vegetation collapse is caused by a strong internal climate variability of droughts and the nonlinear bioclimatic thresholds, rather than a strong positive vegetation feedback and multiple equilibria in the coupled climate–biome system. The implication of the simulated vegetation collapse to the proxy record is also discussed.

The paper is arranged as follows. The model and experimental setup are described in Section 2. Section 3 discusses the simulated evolution of climate-ecosystem changes over northern Africa and its comparison with the observation, while Section 4 investigates the oceanic changes off northern Africa coast and its comparison with the proxy paleoclimate records. A further discussion of the

model–data comparison and its implications are given in Section 5. A summary is given in Section 6.

2. Model and experiment

The FOAM-LPJ is a fully coupled global atmosphere–ocean–land model with dynamic vegetation and without flux adjustment (Gallimore et al., 2005). The coupled atmospheric–oceanic component is FOAM version 1.5 (Jacob, 1997). The atmospheric component, PCCM3-UW (Drake et al., 1995), uses a horizontal resolution of R15 (equivalent to $7.2^\circ \times 4.75^\circ$) and 18 vertical levels. The oceanic component, OM3, uses a z-coordinate and a horizontal resolution of $1.4^\circ \times 2.8^\circ$ and 32 vertical levels (Liu and Yang, 2003).

FOAM is synchronously coupled to the LPJ dynamical global vegetation model (Sitch, 2000; Sitch et al., 2003). The land grid has a horizontal resolution of $1.4^\circ \times 2.8^\circ$. The simulated nine plant function types (PFTs) consist of two tropical trees, three temperate trees, two boreal trees, and two grasses. LPJ's vegetation processes include plant competition, biomass allocation, establishment, mortality, soil and litter biogeochemistry, natural fire, and successional vegetation changes. The detailed coupling between FOAM and LPJ is described in Gallimore et al. (2005). Here, at the request of one reviewer, we describe briefly the coupling scheme for the evapotranspiration. FOAM uses a surface evaporation scheme, which is based on aerodynamic representation that assumes the surface latent heat exchange is proportional to wind speed, a roughness length and stability dependent drag coefficient and the surface to air gradient of specific humidity (Hack et al., 1993). The LPJ surface evaporation is given empirically by an evapotranspiration process with plants (Sitch et al., 2003; Haxeltine and Prentice, 1996), which takes the minimum of two functions: one defining the availability of soil water for root uptake (supply) and the other the availability of light for opening leaf stomata (demand). For FOAM-LPJ, the LPJ evaporation process is used for space occupied by leaf-covered vegetation and the FOAM formulation is used for space covered by leafless vegetation or bare ground.

FOAM captures most major features of the observed global climatology as in most state-of-the-art climate models (Liu et al., 2003a, b). It produces reasonable climate variability, including ENSO (Liu et al., 2000), Pacific decadal variability (Wu et al., 2003), as well as tropical (Liu et al., 2004) and North (Wu and Liu, 2005) Atlantic variability, although the simulated variability, in general, is somewhat weaker than observed. In FOAM-LPJ, the simulated biome distribution has been found to be in reasonable agreement with potential natural vegetation distribution (Gallimore et al., 2005; Notaro et al., 2005). FOAM-LPJ has recently been applied to the study of climate-ecosystem in the Mid-Holocene (Gallimore et al., 2005) and from the pre-industrial to the present (Notaro et al., 2005).

The Holocene simulation is spun up as follows. First, a preindustrial experiment is integrated for FOAM-LPJ for 600 years. Starting from year 102 of the preindustrial run, a Mid-Holocene experiment is performed with the orbital forcing at 6 ka for 400 years. The transient FOAM-LPJ simulation starts from the end of this Mid-Holocene run and is integrated starting from 6.5 to 0 ka with the orbital forcing updated each year following Berger (1978), but all other forcing parameters fixed. No solar variability (other than the orbital change) and volcanic forcing are imposed. This allows us to focus on the role of the gradual orbital forcing on climate evolution. The final state of the transient simulation at 0 ka is close to the end state of the preindustrial run. This suggests that, without flux adjustment, the model climatology and vegetation in FOAM-LPJ do not exhibit significant climate drift during the entire simulation.

3. Transient responses of the North Africa climate-ecosystem

We first study the change of the 500-yr mean climatology from the Mid-Holocene (6–5.5 ka) to the present (0–0.5 ka). At present, the total vegetation cover is confined south of 15–20°N in northern Africa (Fig. 2a), with the northern edge belt dominated by grasses (Fig. 2d). The simulated vegetation cover is more extensive than the present observation (about 5° more northward), because of a wet bias of the FOAM climatology over northern Africa (Fig. 3a). In the Mid-Holocene, the total vegetation cover extends northward by about 500 km across most of northern Africa (Fig. 2b). Therefore, desertification occurs across the southern Saharan region, with the vegetation (Fig. 2c), mainly grasses (Fig. 2f), replaced by desert. In this region, the desertification is accompanied by a significant reduction of the North Africa monsoon, as shown in the reduction of the rainfall and monsoon wind in southern Sahara (Fig. 3b, c).

3.1. The abrupt desertification

A further examination of the vegetation response (Fig. 2c and f) shows that the major vegetation change occurs as an abrupt collapse in the central northern Africa (10–35°E, 17–22°N, area 1 marked in Fig. 2c), where vegetation cover collapses almost completely around 5 ka.[2] This abrupt collapse is seen clearly in the transient evolution of the vegetation cover in Fig. 4a. A separation of the vegetation into tree and grass further shows that the abrupt vegetation collapse is due to grass (Fig. 4b). A small fraction of deciduous trees and shrubs in the Mid-Holocene diminishes gradually with time. In the first 1000 years, the maximum vegetation cover remains near

[2]The dominance of the abrupt vegetation change in area 1 can also be seen in the EOF1 (EV = 37%) of the vegetation cover over northern Africa, whose pattern and time series coincide well with those of area 1.

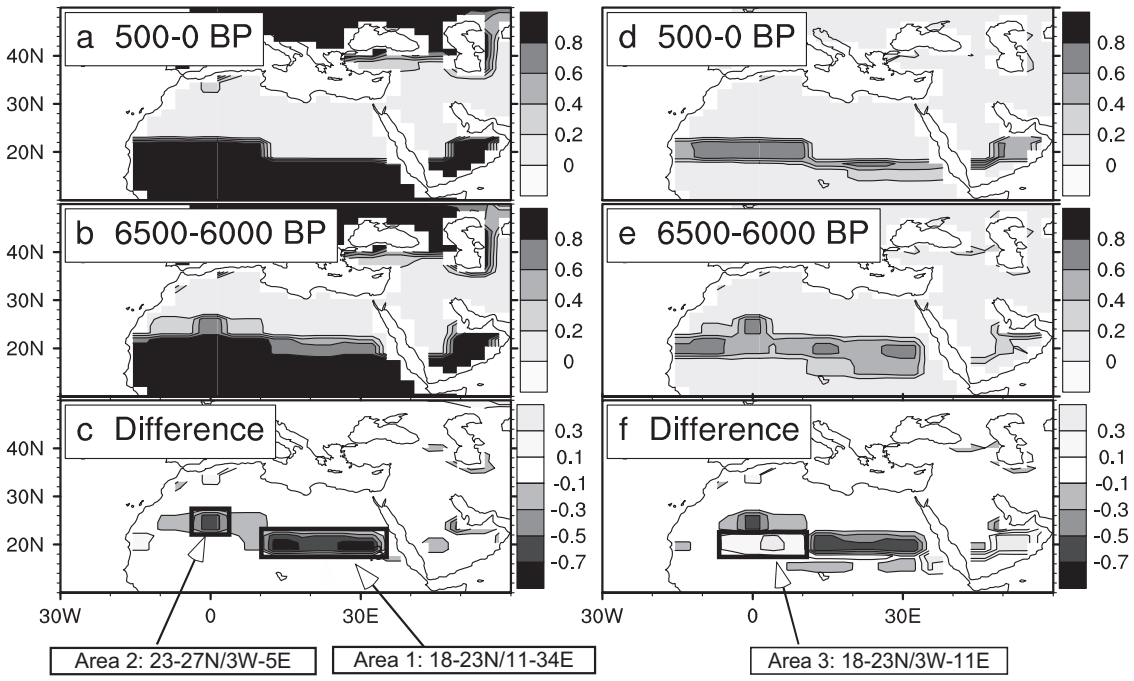

Fig. 2. Total vegetation fractional coverage climatology for (a) the present (0.5–0 ka), (b) Mid-Holocene (6.5–6.0 ka), and (c) the change present—Mid-Holocene. (d)–(f) the same as (a)–(c), but for grasses. The three areas marked in (c) and (f) are referred in the paper as area 1 (11–36°E, 18–23°N), 2 (3°W–5°E, 23–27°N) and 3 (3°W–11°E, 18–23°N).

the level of 0.9, while the climatological (as defined as the 100-yr running mean) vegetation cover decreases linearly from 0.6 to 0.4. At 5.5 ka, the maximum vegetation cover is reduced suddenly to about 0.7 and the climatological vegetation cover shows a first abrupt drop from 0.4 to 0.3. The major collapse event occurs at 5 ka, with the vegetation diminishing almost completely within a century. Later at about 4.6 ka, vegetation exhibits a minor rebound, with the maximum vegetation cover back up to 0.3. The rebound lasts for several hundred years and collapses at about 4.2 ka, after which this area is covered by desert permanently. Interestingly, a similar post-collapse rebound was also observed near 4.2 ka in the eolian dust record from Site 658 (deMenocal et al., 2000; Adkins et al., 2006).

Local climatology also changes substantially during the entire period, with a diminishing rainfall and increasing temperature (Fig. 4c and d), qualitatively consistent with previous time-slice simulations (e.g. Liu et al., 2003a, b). Physically, the weakening of the Africa monsoon rainfall towards the latest Holocene reduces the cloudiness and therefore increases the incoming shortwave radiation and sensible heating. The drier surface also reduces the latent heat release. Both contribute to the gradual warming. However, in contrast to the abrupt vegetation change, the overall change of the local climate is rather gradual in both temperature and precipitation. The temperature shows virtually no abrupt change. The precipitation shows only very subdued anomalies. For example, at 5.5 ka when the maximum vegetation cover exhibits a first reduction, there is no corresponding abrupt change in the climatological precipitation. Later at about 5 and 4 ka, around the times of the major and the final vegetation collapse, there is a detectable abrupt decline of precipitation, but with a much smaller amplitude relative to that of vegetation collapse. Indeed, each precipitation decline is about 20% of the climatological rainfall, much smaller than the complete (~100%) collapse of vegetation cover. Furthermore, these two precipitation declines seem to be comparable with the strong internal variability of precipitation, and therefore may be associated with internal climate variability, instead of vegetation feedback—a point to be returned later.

3.2. Other regional responses

The simulated northern Africa vegetation also exhibits transient responses different from the abrupt collapse in area 1. In a relatively small area in the northern central–western Africa (3°W–5°E, 23–27°N, area 2 in Fig. 2c), vegetation collapses, again due to the grass change. However, different from area 1 (Fig. 4a and b), the collapse of the vegetation in area 2 does not occur until about 3 ka (Fig. 5a and b). In addition, the vegetation collapse is not as abrupt and as complete as in area 1, with the vegetation climatology actually diminishing linearly towards the present. The corresponding precipitation and temperature also change much more gradually (Fig. 5c and d) than in area 1 (Fig. 4c and d).

South of area 2 in a large area 3 (3°W–11°E, 18–23°N, marked in Fig. 2f), vegetation exhibits yet another type of response. Towards the latest Holocene, grass cover increases steadily at the expense of trees, such that the total vegetation remains almost fully covered (Fig. 6a,b).

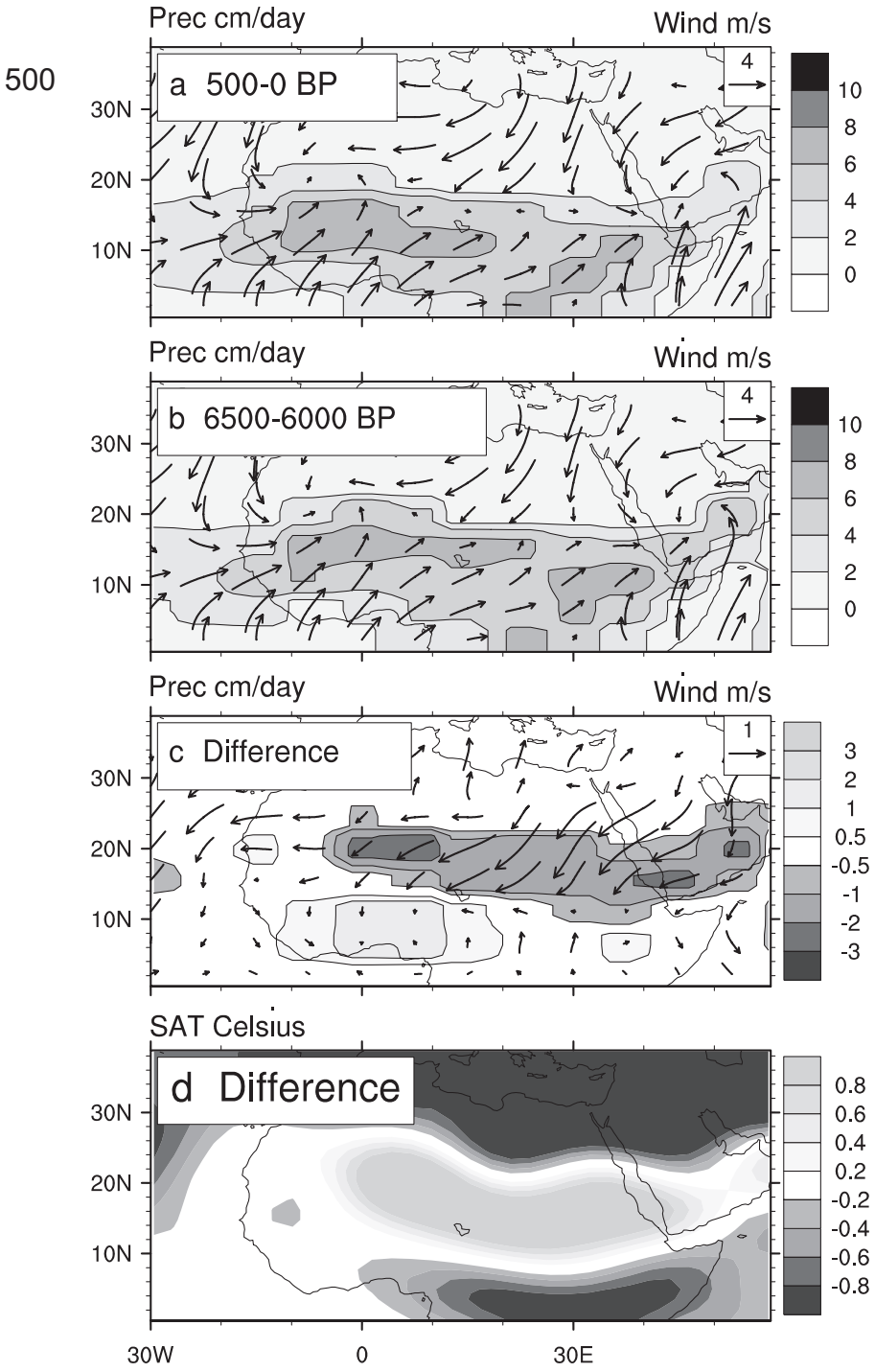

Fig. 3. JJASON mean precipitation and surface wind climatology for (a) present (0–0.5 ka), (b) Mid-Holocene (6.5–6.0 ka), and (c) the change from the Mid-Holocene to the present. (d) Change of annual mean surface air temperature from the Mid-Holocene to the present (similar to (c), but for air temperature).

In the mean time, precipitation decreases and temperature increases, both linearly (Fig. 6c and d).

A comparison of the evolution of climate–vegetation system in different areas shed some lights on the mechanism of vegetation collapse. Areas 1 and 2 are located in the northern edge of the monsoon rain belt. With a climatological annual rainfall of 300–400 mm/yr (Figs. 3b, 4c and 6c), these two regions are the driest areas covered by vegetation in the Mid-Holocene (Fig. 2b and e). In spite of a slightly wetter Mid-Holocene climate in area 1 than in area 2 (400 vs. 300 mm/yr), vegetation declines earlier in area 1, due to a faster decline of rainfall there. In both areas, grass cover collapses when the annual rainfall is reduced to about 250 mm/yr, which takes place around 5 ka

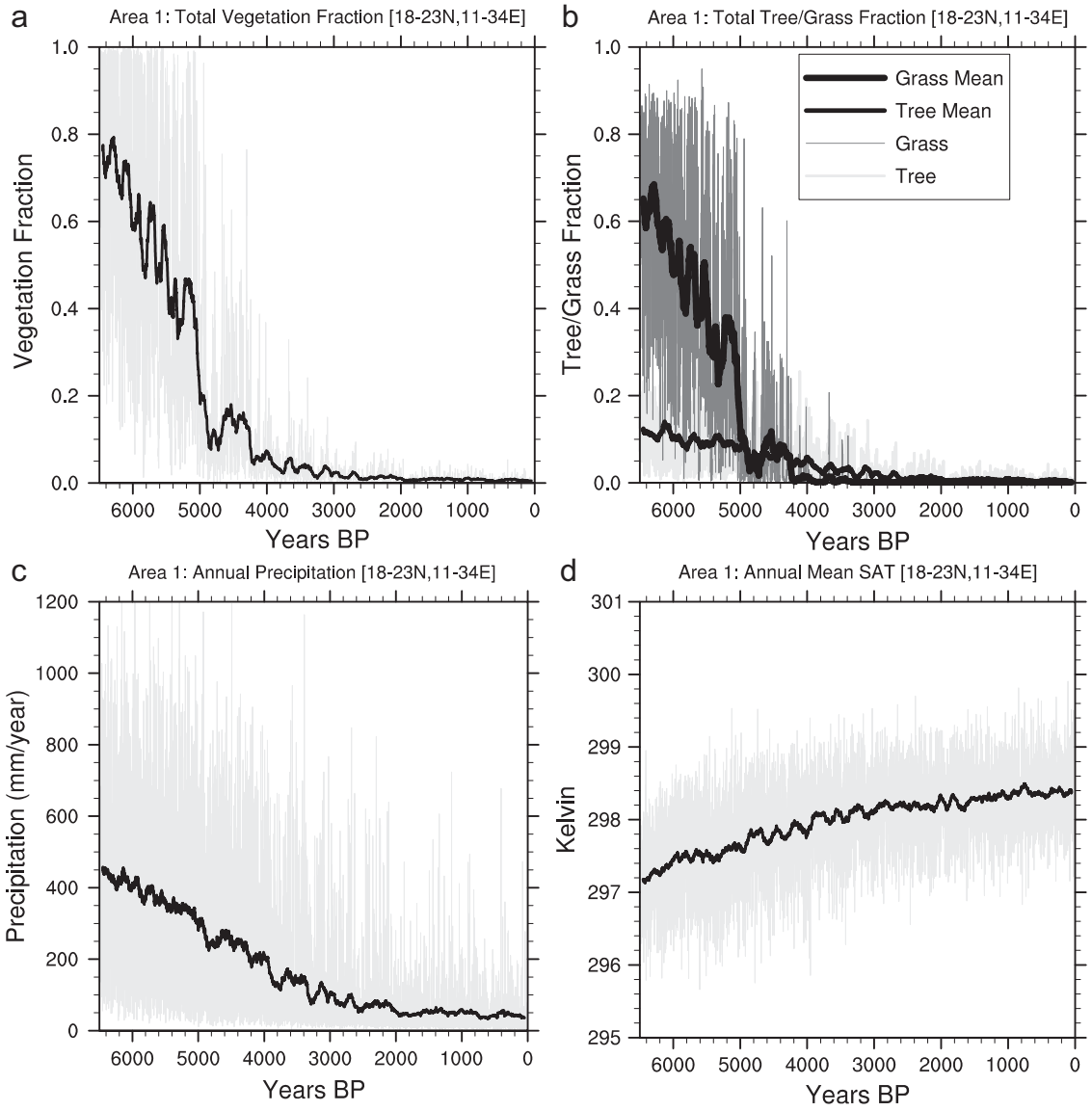

Fig. 4. Area 1 time series of annual (a) total vegetation cover, (b) grass cover and tree cover, (c) precipitation and (d) surface air temperature. Light-thin lines are for annual data and the heavy dark lines for the 100-yr running mean climatology.

in area 1 and 3 ka in area 2 (Figs. 4 and 5). The abrupt vegetation collapse seems to depend most critically on the climatology, interannual variability of precipitation and the precipitation thresholds for vegetation persistence. Further analysis, including off-line LPJ experiments, has suggested that in both regions the grass cover collapses when soil moisture is insufficient to allow the plants to maintain leaves. Additionally, with sufficiently frequent dry years, a negative plant carbon balance leads to the disappearance of grass biomass so that the plants die out. Finally, there is no re-establishment of vegetation from bare ground during the severest drought years, with annual mean rainfall below 100 mm/yr. This lowest threshold also plays some role in the preventing the grass recovering after the collapse, especially in area 1 after 4 ka.

Area 3 presents an interesting contrast to areas 1 and 2. Area 3 has a much higher annual mean rainfall (1400 mm/yr) in the Mid-Holocene (Fig. 6c). The climate dries gradually to 600 mm/yr during the latest Holocene. In spite of significant interannual precipitation variability, annual precipitation never drops below 300 mm. During the aridification, tree cover is gradually replaced by grasses, but the total vegetation cover remains little changed. Before 3 ka, the rainfall is sufficient to support a full vegetation cover even during dry years. The gradual drying leads to a favorable condition for grasses relative to trees as a result of competition for soil moisture, the grasses being more effective than woody plants in extracting moisture from the soil surface layers (Sankaran et al., 2005). After 3 ka, the mean climate dries sufficiently such that rainfall can be lowered below the threshold required to support a complete vegetation cover during drought years (about 500–600 mm/yr in this region), leading to episodic vegetation reductions.

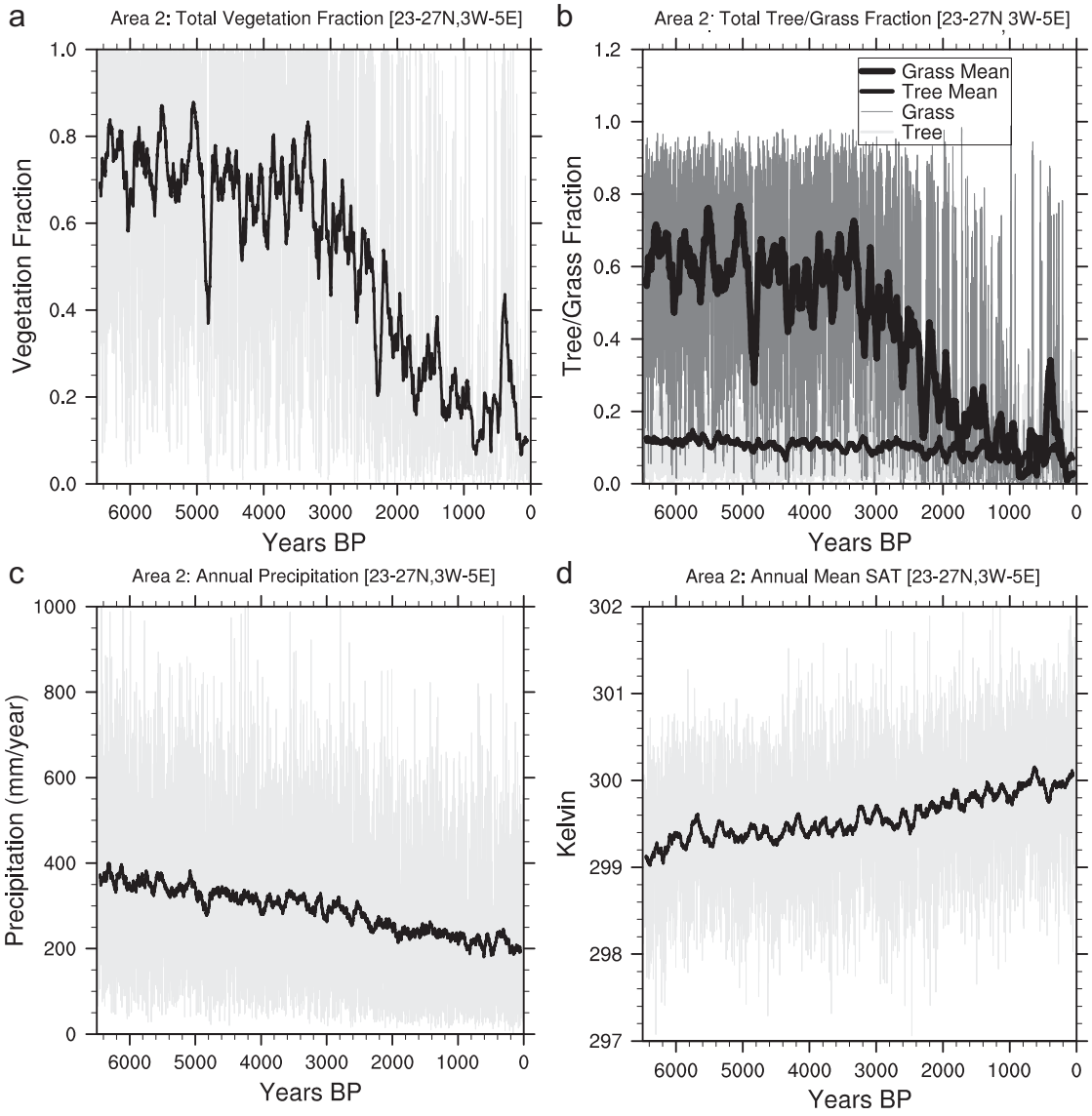

Fig. 5. Time series the same as Fig. 4, but for area 2.

3.3. *Vegetation feedback and the mechanism of abrupt change*

The simulated major collapse of vegetation cover in area 1 is not caused by a strong positive vegetation feedback on climate. This is in contrast to previous studies, in which a strong positive vegetation feedback was considered to be critical for the collapse of the climate–biome system (C99; Brovkin et al., 1998, 2002). Detailed discussions on the vegetation feedback and the mechanism of the abrupt change in the Holocene simulation are beyond the scope of this paper and are reported elsewhere (Liu et al., 2006a; Wang et al., 2007; Notaro et al., 2007). For completeness, here, we discuss the feedback and the mechanism of abrupt change briefly.

The lack of a strong positive vegetation feedback on annual precipitation is implied in the gradual precipitation decline accompanying the abrupt collapse of vegetation cover (Fig. 4). As noted in Fig. 4 above, the precipitation decline accompanying the completely vegetation collapse is less than 20% in our simulation, much smaller than the over 40% precipitation reduction in C99. Furthermore, the precipitation reduction is much smaller than internal variability in C99, but is comparable with internal variability in our simulation. Therefore, the precipitation reduction has to be caused by a strong positive vegetation feedback on annual rainfall in C99, but can be caused by internal climate variability in our simulation.

The lack of positive vegetation feedback in the Mid-Holocene is further confirmed with a statistical assessment following the method of Liu et al. (2006b). Indeed, the statistically estimated feedback of vegetation cover on annual rainfall in region 1 is negative in the Mid-Holocene (Notaro et al., 2007; Wang et al., 2007). This negative vegetation feedback on annual rainfall is further confirmed by explicit dynamic experiments in FOAM-LPJ.

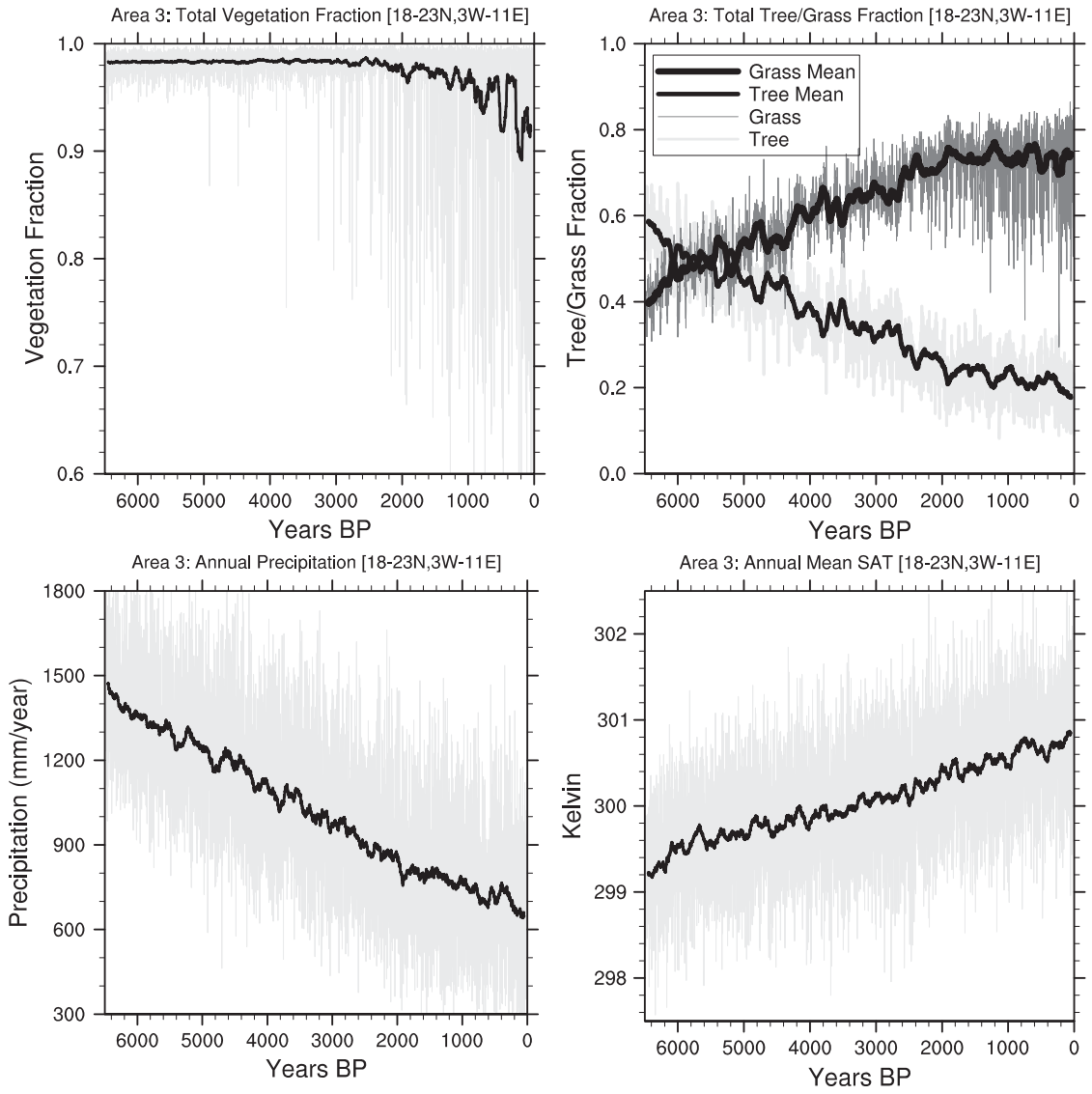

Fig. 6. Time series the same as Fig. 4, but for area 3.

This negative feedback is found to be caused by the competition between grass transpiration and bare ground evaporation in the monsoon season in the Mid-Holocene; surface albedo has a small impact in the model, because of the small albedo difference between grassland and wet soil (Notaro et al., 2007).[3] Therefore, the abrupt vegetation collapse cannot be attribute to a positive vegetation feedback on rainfall in our model.

[3]Two more notes on the vegetation feedback. First, the negative vegetation feedback on annual rainfall reverses to positive towards the Late Holocene. Second, for monthly variability involving only leaf phonology, the statistical assessment shows a robust positive vegetation feedback on rainfall in FOAM-LPJ for the present (Liu et al., 2006b) and Mid-Holocene (Wang et al., 2007). The dependence of vegetation feedback on time scale is reminiscent of the grassland-precipitation feedback estimated using another statistical method for the southwest United States, which shows a reversal from monthly to annual time scales (Wang et al., 2006). The complex nature of climate–vegetation feedback needs much further study.

The variety of abrupt changes of the Holocene simulations in our model and previous models can be understood from a unified viewpoint, as proposed recently by Liu et al. (2006a). The classical abrupt change, as proposed by Claussen (1998) and Brovkin et al. (2002), occurs through the so-called "unstable collapse" associated with a multiple equilibria of the climate-ecosystem. With a gradual declining of the insolation forcing, the coupled system collapses from a green equilibrium state to a desert equilibrium state via an unstable intermediate state. A strong positive vegetation feedback is required to produce the multiple equilibria; this positive feedback also requires a large collapse of vegetation to be accompanied by a large collapse of precipitation. If the positive vegetation feedback is not sufficiently strong, the coupled system only has a single equilibrium. Except for two cases, now, the coupled system usually decreases rather smoothly as a "stable decline," as in Brovkin et al. (2002) and Wang et al. (2006). The first exception is trivial, in which

vegetation feedback is marginally strong such that the coupled system is near its neutral stability. Now, the "stable decline" approaches the "unstable collapse" and appears as a rather abrupt decline. This is the case for C99. This near-neutral collapse, in principle, is the same as the "unstable collapse." The second exception is nontrivial and involves climate variability. If soil moisture has substantial decadal variability that is forced by internal climate variability, vegetation can collapse suddenly when the climatological precipitation exceeds bioclimatic thresholds such that the vegetation is pushed into the large "attractive well" of the desert equilibrium state. This is called the "stable collapse" (Liu et al., 2006a). The stable collapse depends critically on low-frequency variability forcing, instead of a strong positive vegetation feedback, and, therefore, a collapse of vegetation is not necessarily accompanied by a strong collapse of precipitation. The vegetation collapse in our model resembles a stable collapse, because of the weak vegetation feedback and the large rainfall variability (Fig. 4).[4]

3.4. Comparison with data

Proxy data are in general agreement with the two most distinct features of the northern Africa desertification in the Holocene simulation: the occurrence of large-scale abrupt changes in the Mid-Holocene, and a variety of evolutions in different regions (see recent syntheses on environmental changes in northern Africa and references therein, e.g., Gasse, 2000, 2002; Gasse and Roberts, 2004; Hoelzmann et al., 1998; Hoelzmann et al., 2004; Kuper and Kropelin, 2006). The best-dated Holocene lake and pollen records are located in Fig. 7, where sites cited in the text and figures are numbered S1, S2…. Here, we will focus on the overall features, while a more detailed discussion is presented in the Appendix A. During the Early Holocene, spectacular hydrological and vegetation changes occurred between 13°N and 21°N, in the present-day semi-arid Sahel and the arid southern Sahara. This zone well coincides with the simulated belt of maximum decrease in rainfall since 6.5 ka (Fig. 3c). Terrestrial data reveal a southward shift of rainfall and vegetation belts towards the latest Holocene (Kuper and Kropelin, 2006). The modern tropical vegetation zones (from South to North: the Guinean forest, the Sudanian savanna woodlands, the Sahelian pseudo-steppe, and desert-type vegetation), and the steep gradient of summer precipitation, which occurs today at the Sahel–Sahara fringe have been displaced southward by 4–5° latitude. The position of the 400 mm isohyet has been estimated for the Mid-Holocene to be at 19°N in the eastern Sahara (S1; Ritchie and Haynes, 1987) and at 21°N in the western Sahara (Lézine, 1989), relative to about 14–16°N at the present. The monsoonal origin of rainfall

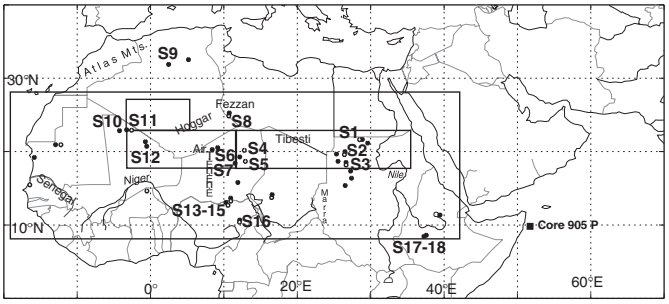

Fig. 7. Location map of the best-dated terrestrial sites. See Hoelzmann et al. (2004) for detailed information and original references on these sites. S1, S2…. are sites illustrated in Figs. 1 and 12 or cited in the text. Black circles: lake records; open circles: paleovegetation records. S1: Selima Oasis; S2: Oyo; S3: El Atrun; S4–S5: Ténéré Desert; S6: Bilma; S7: Fachi; S8: Wadi Teshuinat; S9: Hassi el Mejnah; S10: Taoudenni-Agorgott; S11: Wadi Haijad; S12: Ine Kousamene; S13: Bougdouma; S14: Kajemarum Oasis; S15: Lake Bal; S16: Lake Tilla; S17: Lake Tilo; S18: Lake Abiyata. Large rectangle: area of lake-level data compilation showed in Fig. 1b. Small rectangles: areas 1–3 described in the model as in Fig. 2.

south of ca 19–22°N is demonstrated by paleovegetation evidence and by the isotopic composition of both groundwater and lacustrine carbonates. Few data are available in the northern Sahara. Desert-type vegetation occurred at 25°N in southern Libya (S8, Fig. 7) and at 22°5′N in southern Egypt (in Hoelzmann et al., 2004). At the northern fringe of the western Sahara (S9), Holocene lakes desiccated rapidly after 5.5–4.8 ka (Gasse, 2002). Although this area may have been supplied by rainfall of extra-tropical origin (Gasse and Roberts, 2004), it has contributed to the dust influx to the ocean via NE trade winds. Conditions close to modern prevailed everywhere after 4–3 ka, although minor positive oscillations in precipitation have been inferred at some sites. Between ~8 and 4–3 ka, a mosaic-like pattern in lake level and vegetation appears when climate became unstable and when local and site-specific characteristics become more important (Lézine and Casanova, 1989). As a whole, the climate deterioration appears generally more abrupt in Areas 1–3 than southward. Between ca 16°N and 10°N, the desertification started much earlier and ended much later than 5.5 ka, and is more consistent with Fig. 6 than Fig. 5 (see Appendix A).

Marine dust records, regarded as reflecting climate changes over large parts of the continent, suggest geographical differences in the timing of aridification. An abrupt shift in dust content around 5500 yr BP off the west coast of the North Africa at Site 658 (deMenocal et al., 2000; Fig. 1b) has been attributed to an abrupt aridification and deterioration of the vegetation cover over NW Africa There is strong support from molecular biomarker results at Site 658 that the dust flux increases during the Late Holocene dry period were due to reductions in vegetation. The plant wax abundances (*n*-alkanes) and pollen go very low for the dry periods, suggesting that vegetation cover was also reduced during these times (i.e. not just stronger transporting winds, see Zhao et al., 2003). Dust borne radiogenic isotope records off Somalia suggest an

[4]Low-frequency variability is critical here. Otherwise, strong high-frequency variability suppresses the collapse of the climate-ecosystem (Liu et al., 2006a). This is the case of Renssen et al. (2003).

aridification in two steps in the northeastern Africa, the first one at ~8.5 ka, and a more progressive step from 6 to 3.8 ka (Jung et al., 2004; Fig. 1f).

Overall, regional paleoclimate evidence over northern Africa appears to suggest that, taking into account the whole Sahara–Sahel, the abrupt shift at 5.5 ka observed off the west coast of northern Africa is a major feature of the North Africa climate-ecosystem. The relatively progressive aridification trend from 6 to 3.8 ka suggested by dust records off Somalia also appears to be a significant feature. The former appears to be a good recorder of changes in the southern Sahara and perhaps Northwest African monsoon (16–20–22°N), while the latter reflects more a gradual change of the southern Sub-Saharan areas and the SW Indian monsoon (Abell and Hoelzmann, 2000; Fleitmann et al., 2003; Jung et al., 2004). While the abrupt vegetation collapse is clearly a major feature of the Holocene aridification in northern Africa, especially in the southern Sahara, the evidence of abrupt collapse of large-scale precipitation is less clear. In the semi-desert region, even if the precipitation decreases gradually, a sudden replacement of grasses with desert will allow the wind to entrain and transport much more dust towards the Atlantic, leading to the sudden increase of dust flux there. Furthermore, there is also significant evidences for less robust and less abrupt changes in paleovegetation and paleohydrological changes over the northern Africa These features are in qualitative agreement with the model simulation, and will be considered further in light of the oceanic responses below.

4. Transient responses of the North Atlantic Ocean–atmosphere system

4.1. Simulation of the evolution of SST and upwelling

Towards the latest Holocene, the simulated annual mean SST change exhibits a basin-wide dipole pattern, with a warming in the tropics and a cooling north of 20°N (Fig. 8a). This large-scale SST change is determined mainly by the surface heat flux (Liu et al., 2003b). In particular, the annual mean insolation forcing increases in the tropics and decreases in the extratropics due to the decreased obliquity.

Seasonal responses are much larger than the annual mean for SST and surface wind (Fig. 8b–e), and are consistent with earlier studies (e.g. Liu et al., 2003a). The summer monsoon wind is reduced towards the present, which leads to a southward retreat of the ITCZ and an enhanced northerly wind over the North Africa (Fig. 8d). The SST change is similar to the annual mean with a dipole anomaly of a modest amplitude. The reduced meridional SST gradient has been suggested to act as a positive oceanic feedback on the monsoon reduction (Kutzbach and Liu, 1997). The wind change in fall is similar to summer, but the SST exhibits a strong cooling basin-wide (Fig. 8e). This strong cooling results from the peak insolation reduction in early fall (from 6 to 0 ka), and a further delay by the thermal inertial of the ocean. As a result, the SST pattern differs significantly between summer and fall, while the wind response remains similar over the tropical Atlantic. Nevertheless, the SST gradient remains negative northward as in summer, suggesting that the positive oceanic feedback on monsoon lasts from summer into fall. In winter (Fig. 8a), the anomalous insolation heating lowers the surface pressure over the North Africa continent, which leads to a southward geostrophic wind over the subtropical western Atlantic and an anomalous convergence from the tropics towards the continent. The SST change, however, exhibits a modest dipole as in summer, in spite of significantly different wind responses in the tropics. The wind response is weak in spring (Fig. 8c), while the SST exhibits a strong basin-wide warming. The disparity between the seasonal changes of wind and SST is an indication that the overall change of large-scale SST pattern is forced predominantly by insolation forcing and surface heat flux forcing.

Upwelling reinforces the surface heat flux in certain seasons and regions, but counters the heat flux forcing in other seasons and regions. North of 20°N, the enhanced northerly wind along the west coast enhances the coastal upwelling during the latest Holocene (Fig. 9), reinforcing the subtropical cooling along the coast of western North Africa Over most of the tropics (south of 20°N), SST increases because the anomalous upwelling cooling is overwhelmed by the anomalous surface flux heating (Fig. 9).[5]

Now we focus on the evolution of SST along the west coast of North Africa near Site 658. The SST cools only slightly in the annual mean (~0.1 °C, Fig. 10a) because the site is located near the nodal line of the annual mean SST dipole (Fig. 8a) (but see discussions later). The seasonal SST changes are much larger, with a decrease of 1 °C in the warm season (fall) and an increase of 1 °C in the cold season (spring), consistent with the strong basin-wide monopole SST change in those two seasons (Fig. 8e and c). Physically, towards the present, the seasonal cycle of insolation forcing is reduced significantly, which reduces the seasonal cycle of SST, but has little impact on the annual mean SST. In contrast, the northerly wind along the western Africa coast (Fig. 10b) is enhanced in all the seasons towards the latest Holocene. The northerly is enhanced the most in fall, because of the southward migration of the Africa monsoon, and, in turn, the trade wind system (Fig. 8e). Northerly winds are also enhanced in winter and spring because the anomalous surface heating over the Northern Hemisphere lowers the surface pressure over the North Africa continent, forcing an anomalous southward geostrophic wind along the west coast of N. Africa, as discussed in Fig. 8b and c. The year-round

[5]On the equator, annual upwelling is reduced towards the present, because of the convergence wind towards the North Africa (Fig. 8a), which is caused by the winter atmospheric response (Fig. 8d). The reduced upwelling reinforce the surface heating and favors a SST warming there.

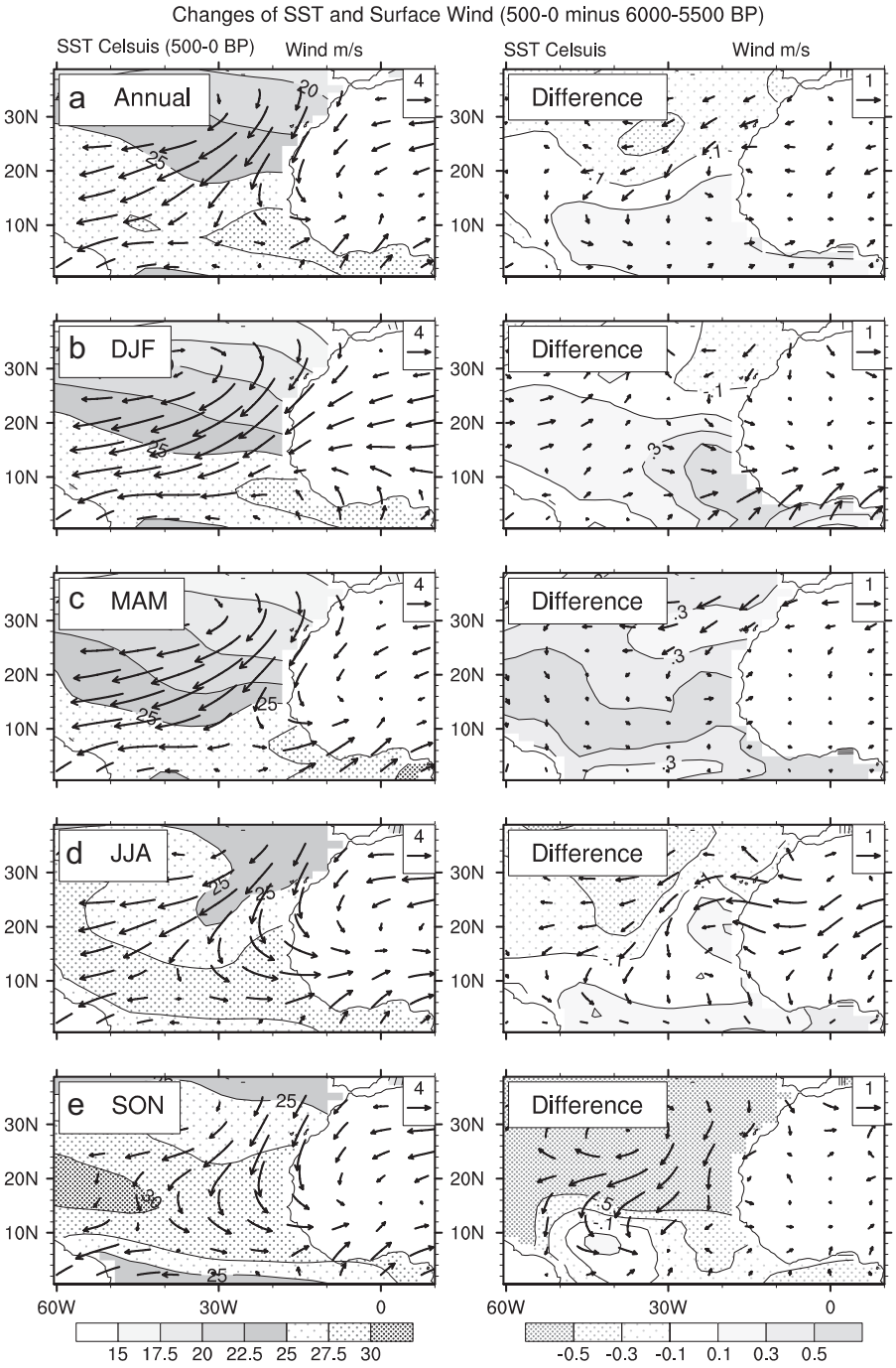

Fig. 8. Changes of SST and surface wind for (a) annual mean, (b) winter (DJF), (c) spring (MAM), (d) summer (JJA) and (e) fall (SON). The left column is the modern climatology (500–0 ka) while the right panel is the difference of the modern and Mid-Holocene (6000–5500 ka).

increase of northerly wind enhances the coastal upwelling in all the seasons (Fig. 10c), which then reinforces the surface heat flux induced cooling trend in the fall, but cancels part of the surface heat flux induced warming trend in winter and spring. The opposite upwelling effects on heat flux forcing between fall and spring may have contributed to the asymmetric SST evolution, with a fast surface cooling in fall and a relatively slower warming in spring (Fig. 10a). Overall, the coastal upwelling cooling may have contributed to the annual mean cooling substantially. This upwelling effect, however, may have been significantly underestimated because of the coarse resolution ocean model here.

4.2. Comparison with data

The simulated annual mean cooling and enhanced upwelling is consistent in sign with the reconstruction of alkenone SST and opal flux (a proxy for upwelling, Adkins et al., 2006) (Fig. 11) at Site 658C (20°45′N) and further

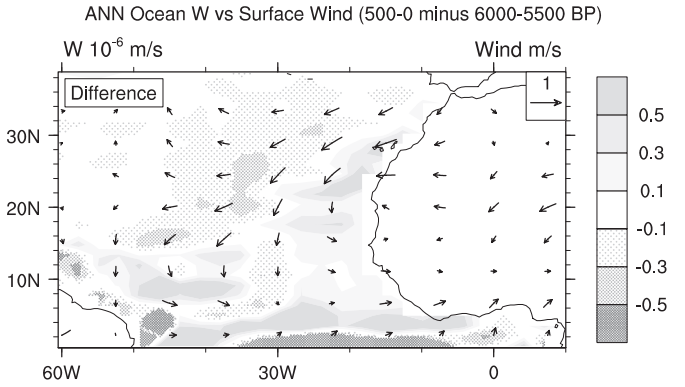

Fig. 9. Changes of the annual surface wind and upwelling climatology from the Mid-Holocene (6–5.5 ka) to the present (0.5–0 ka). Upwelling is represented by oceanic vertical velocity at the depth of 50-m.

north in the Iberian Margin at Site SU8118 (37°46′N, 10°11′W) (Bard et al., 2000), MD952042 (37°45′N, 10°11′W) and MD952040 (40°35′N, 9°52′W) (Pailler and Bard, 2002). The simulated cooling is about 0.1 °C at 658C and over 0.3 °C against the coast near the two sites of Iberian Margin. The magnitude of the cooling is smaller than the reconstructed cooling of about 1 °C. The smaller cooling in the model could be contributed by the coarse model resolution, which tends to underestimate the effect of coastal upwelling on SST. The smaller model annual mean cooling at Site 658C could also be caused by a model bias. This site is located near the node line between the warm tropics and cold extratropics (Fig. 8a). The Inter-tropical Convergence Zone (ITCZ) in the FOAM climatology is biased northward by perhaps up to 5° over the land and the coastal region (Fig. 3a). Therefore, the model Site 658C should be located further north by about 5°, where the annual mean SST cooling should be more significant, with a magnitude of about 0.2 °C in the model.

The simulation has some implications to the interpretation of the proxy records. First, the much large seasonal signal than the annual signal implies that the proxy reconstruction could be biased towards the strong seasonal signal in fall. This notion, however, counters the observational study that the alkenone SST in this region really resembles the annual SST (Müller and Fischer, 2001). Second, the simulation also suggests that upwelling may not be the dominant forcing of the coastal SST, because the upwelling effect tends to be overwhelmed by the heat flux forcing in some seasons. This suggests that one has to be cautious in interpreting the relation between SST and upwelling in paleoclimate changes, especially for orbital time-scale changes, because the insolation forcing can exert a strong shortwave forcing on SST, which may overwhelm the upwelling effect, as discussed in Figs. 8 and 10.

Finally, there may still be some uncertainties on the SST reconstruction itself. An earlier SST reconstruction using foram transfer function even shows a strong Late Holocene warming on this site, opposite to the modest cooling trend

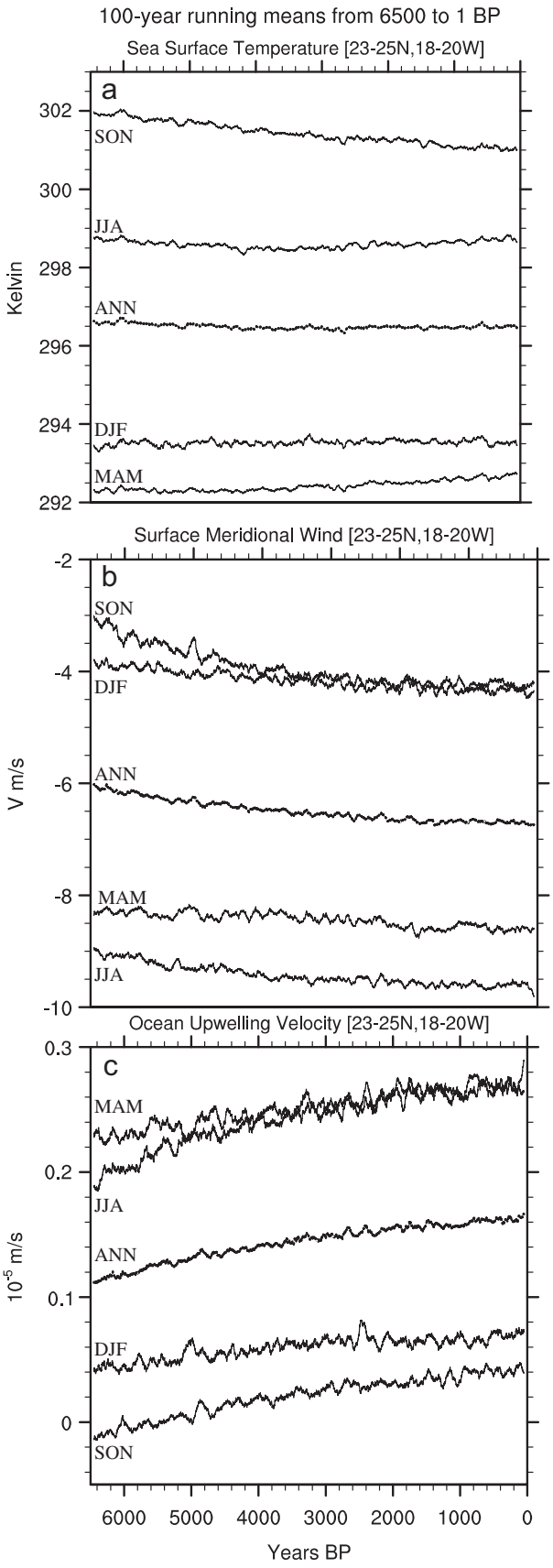

Fig. 10. Evolution time series of the climatology (100-yr running mean) of winter (DJF), spring (MAM), summer (JJA), fall (SON) and annual mean (a) SST, (b) meridional surface wind and (c) upwelling (50-m) velocity near the site 658C (18–20°W, 23–25°N).

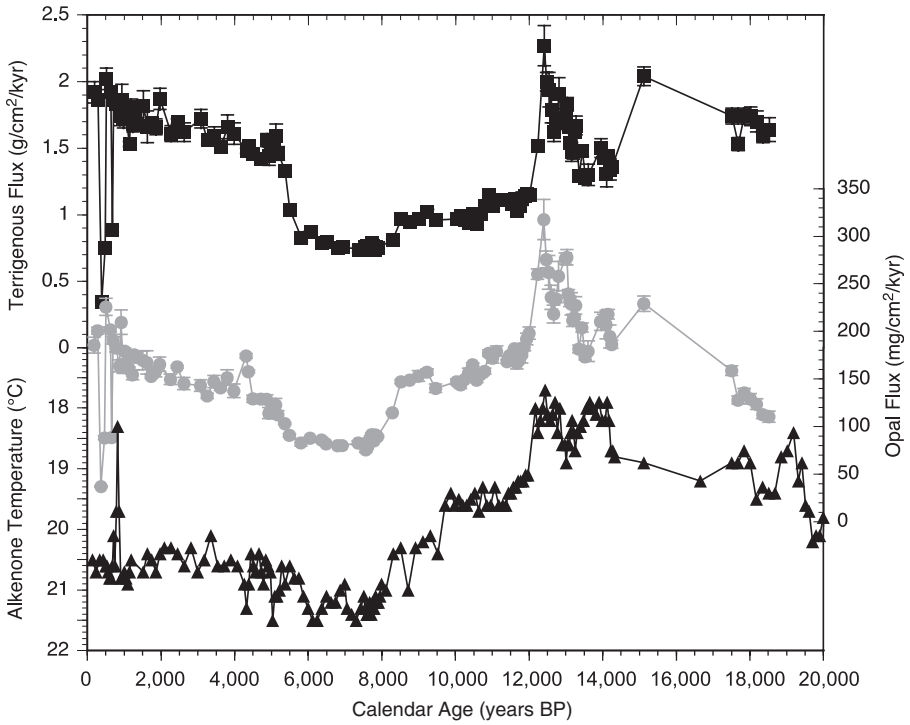

Fig. 11. Marine record on Site 658C. Alkenone SST (a proxy for annual SST), opal accumulation flux (a proxy of upwelling), and terrigenous accumulation flux (dust flux) since the LGM. The SST cools by about 1 °C from the Mid-Holocene to the latest Holocene, and is accompanied by an increased upwelling. The change of the SST and upwelling, however, are much more gradual than the sudden increase of dust in the Mid-Holocene (at about 5 ka). (Adapted from Adkins et al., 2006).

from the alkenone SST (Fig. 9 of Adkins et al., 2006). At Site 658 this discrepancy is likely due to ecological influences on the foram assemblages and SST transfer function estimates. The warmer Late-Holocene transfer function SSTs at Site 658 were associated with greatly increased foram size and increases in *G. bulloides* abundances, which depends on nutrient supplies, foram size and upwelling dynamics. Overall, we tend to think that the Late Holocene cooling trend inferred from the alkenone SST at Site 658 is valid. The amplitude is about 0.5–1.0 °C in annual mean, probably weighted to the max upwelling season response though. The model response also appears to be in the same sign, but too weak in the magnitude.

5. Discussions

5.1. Implication to the abrupt change

We now further explore the implications to the abrupt change in Northern Africa in light of the synthesis of the coupled ocean–atmosphere-vegetation proxy evidences as well as the model simulation. Combining the terrestrial and marine proxy data together, it appears that the abrupt collapse of dust flux at Site 658C of centennial time scale is a distinctive feature related to an abrupt collapse of vegetation cover in the southern Sahara region. However, there are less clear evidences of an equally sharp abrupt change in climate, such as the precipitation, temperature and wind. Indeed, in the same core of Site 658C, opal flux increases and alkenone SST decreases since the Mid-Holocene, but both seem to change rather gradually from 6 to 4 ka (Fig. 11, Adkins et al., 2006). Since these two datasets are from the same core, the time resolution is unlikely to be much different from the dust flux. Since the opal flux is a proxy for upwelling, and in turn the northerly wind, we may then infer from the opal flux and alkenone SST that the wind and SST at Site 658C does not exhibit a collapse as abrupt as the dust flux. Therefore, it is possible that the abrupt collapse of dust flux is more due to the collapse of the vegetation cover than the precipitation field itself. In addition, over the North Africa continent, proxy evidences seem to suggest a significant drying trend after the Mid-Holocene, but seems to exhibit a less abrupt collapse than the dust flux at 658C (Figs. 1c, d). There are also geographical differences in the timing and rate of aridification (Appendix A). There are also continental proxy records that seem to correspond well to the marine record off the coast of Somali, which indicates a more progressive drying trend (Fig. 1f).

Our model simulation shows much more clearly an abrupt collapse of North Africa ecosystem in response to a relatively gradual climate change, including oceanic changes, in the Mid-Holocene. As a result, the model vegetation collapse is likely to be caused mainly by a nonlinear vegetation response to bioclimatic threshold. The rainfall threshold depends primarily on the mean

climatological rainfall, but also on the intensity of multi-year climate variability, because both are important in determining the minimum precipitation threshold for vegetation survival and establishment. In contrast to C99, vegetation feedback does not play a dominant role in the vegetation collapse in our model.

It is possible that the abrupt change in climate accompanying the vegetation collapse is underestimated in our model. For example, while our model shows virtually a linear trend response in SST and upwelling with a small magnitude (Fig. 10), the reconstruction exhibits a transition with a relatively larger amplitude from 6 to 4 ka than in later years (Fig. 11). One possibility is that the region of abrupt vegetation collapse is too small in our model, because the model still underestimates the climatological response of the northern Africa climate-ecosystem (Fig. 2 and 3) relative to proxy evidences. This underestimation of the response of monsoon climatology is one common feature of many previous GCM simulations, perhaps due to the underestimation of internal feedbacks. (However, a comparison of the statistical assessment of vegetation feedback on monthly precipitation does not show a weaker vegetation feedback on local precipitation in the model than in the observation (Liu et al., 2006b).) It is also possible that the smaller change of monsoon system is caused partly by the wet bias of the model climatology, which leads to an overproduction of vegetation cover at the present. Clearly, this issue remains to be further explored.

5.2. Implications of the strong interannual variability on proxy evidences

There are several high-resolution records documenting large climate instability, especially in ecotone areas and during the aridification episode when the systems become more sensitive to minor climate changes. The model variability is in general consistence with the increased environmental variability during the Holocene desiccation trend. This trend, which started as soon as 8–7 ka in many areas, is not linear. For example, in the NE Sahara (S2, Fig. 7), rapid and frequent oscillations of tree pollen percentages are observed from ca 7.5 to 5.5 ka during the southward retreat of the tropical savanna from 19°N (Fig. 12b; see the Appendix A for details). Large vegetation and hydrological fluctuations after 7.5–6 ka are also inferred in existing waterbodies of the Sahel, e.g., at site S14 (Fig. 7), from pollen, diatom, and geochemical evidence (Fig. 12c; see the Appendix A for details). The Ethiopian lakes Abiyata (Fig. 1e; S18, Fig. 7) and Tilo (Fig. 12d; S17, Fig. 7), which depend on both the African and the Indian monsoons, also recorded an extreme variability in the precipitation minus evaporation balance after 5 ka.

Most continental proxies in the Sahara/Sahel region, however, do not have a resolution to resolve interannual or even interdecadal variability, a characteristic of tropical climate. Most records register mean environmental conditions at the centennial or even longer time scale. The strong short-term variability (relative to its long-term climatology) in vegetation cover and precipitation (such as in region 1 in Fig. 4), or in the water table, may have important implications to the interpretation of the proxy data. For example, suppose the resolution of each time slice of a pollen record is one hundred years. The identification of pollen at a certain time slice may reflect either the long term vegetation climatology, or an episodic presence of vegetation of years or decades. In the former case, the pollen record should track the vegetation climatology, such as the 100-yr running mean climatology in Fig. 4a, while in the latter case, it should be represented by the maximum vegetation cover envelope in Fig. 4a. These two representations could have different temporal evolution features, the former exhibiting a more gradual change than the latter. Similar situation also applies to the reconstruction of lacustrine conditions.

6. Summary

We performed the first transient simulation of the last 6500 years in a synchronously coupled global general circulation atmosphere–ocean-dynamic vegetation model. The model simulates a variety of vegetation changes in northern Africa The most distinct feature is a major vegetation collapse over the southern Sahara region at 5 ka, consistent with the dust records in marine sediment (deMenocal et al., 2000). In comparison, the simulated precipitation change is much more gradual than the vegetation, implying the absence of a strong positive vegetation feedback. A gradual surface cooling and intensification of upwelling are also simulated along the northern North Atlantic coast, consistent with proxy records there (Bard et al., 2000; Adkins et al., 2006). The extratropical cooling at this site seems to be dominated by the insolation forcing, but is also enhanced by the upwelling cooling. Combining data with model, we speculate that the abrupt change at 5 ka reflects more the collapse of vegetation cover in response to bioclimatic threshold than the abrupt change of the climate field itself. We caution, however, that the climatic response and climate feedbacks may have been underestimated in our model, because of its coarse resolution and wet climatic bias over the northern Africa region.

In addition to this 5 ka abrupt change, our model also simulated different vegetation evolutions. This variety of vegetation evolution is also consistent with paleo proxy evidences of different evolution behavior in the northern Africa It is therefore conceivable that, in addition to a major collapse at about 5 ka, the northern Africa climate-ecosystem experienced a variety of evolutions in the Holocene.

The mechanism of the abrupt change remains to be better understood. The strong interannual climate variability, and the threshold response of the vegetation and its interaction with the climate, has made it challenging to

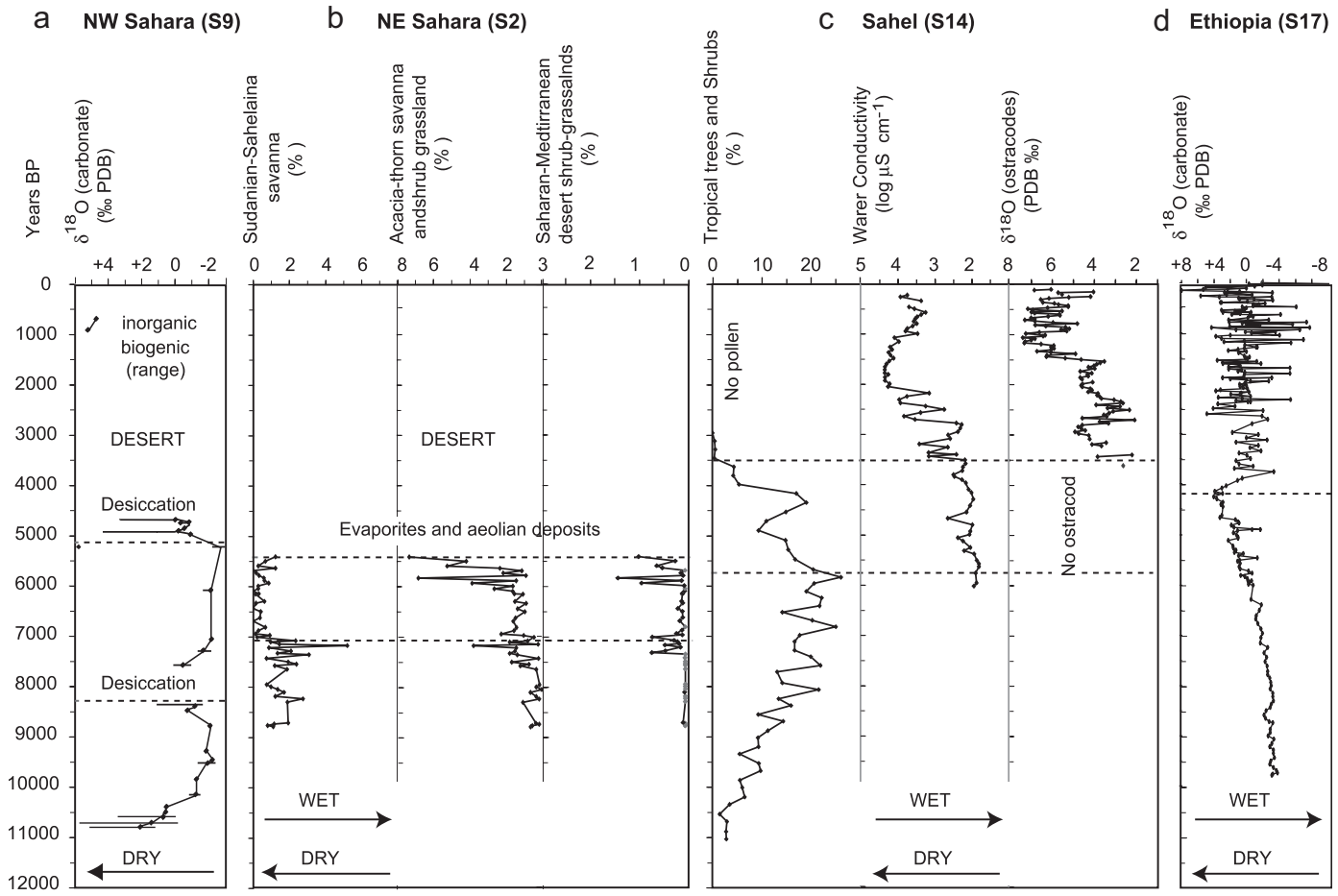

Fig. 12. Examples of Early-mid to Late Holocene shifts from wet to dry conditions. See Fig. 7 for site location. (a) Northeastern Sahara (Hassi el Mejnah, S9; 31°40′N, 2°30′E): $\delta^{18}O$ profile of authigenic inorganic and biogenic carbonate. The range of the later indicates interannual variability (Gasse et al., 1990; Gasse, 2002). (b) Northeastern Sahara (Oyo paleolake, S2; 19°17.7′N, 26°27.6′E; after Ritchie et al., 1985; Ritchie, 1994). Phytogeographic pollen groups. From left to right, percentage of total pollen sum of Sudanian deciduous savanna, Saharo-Sahelian trees and shrubs, Saharan and Mediterranean taxa. The pollen spectra is dominated by Gramineae and Cyperaceae with a sharp shift in the relative proportion of these two elements around 7.5–7 ka, possibly caused by a lake level lowering producing a larger marginal marshy zone. (c) Western Sahel (Kajemarum oasis, S14; 13°22′N, 11°01′E). From left to right: percentage of total pollen sum of tropical savanna and Sahelian trees and shrubs (after Salzmann and Waller, 1998); the pollen spectra is dominated by herbs, the upper part of the profile is devoid of pollen. Diatom-inferred conductivity (Gasse, 2002). $\delta^{18}O$ of ostracod carbonate (*Limnocythere inopinata*) (after Holmes et al., 1998, 1999). (d) d18O profile of authigenic carbonates at Lake Tilo (Ethiopia, 7°03′45″N-38°40′45″E) (Lamb et al., 2000). The dashed lines mark the major desiccation steps.

isolate the causality unambiguously. The strong internal variability also has a strong impact on the timing of the abrupt vegetation collapse.[6] It is also important to interpret the proxy records in the context of climate variability. Stimulated by this simulated vegetation collapse, a conceptual climate–vegetation model study (Liu et al., 2006a) shows that a coupled system without a strong positive vegetation feedback (and the associated multiple equilibrium) can still exhibit abrupt vegetation collapse if it is forced by strong decadal climate variability. This so-called "stable collapse" differs fundamentally from the unstable collapse of C99 in that the former does not require a strong positive vegetation feedback and therefore the vegetation collapse is not accompanied by a strong precipitation collapse, as in the case of our Holocene simulation. In this regard, it is important to expand the observational dataset of high-resolution paleohydrological proxies. Only a synthesis of large scale high-resolution proxy data can help us distinguishing the relative phase and magnitude of the abrupt changes of large-scale vegetation and rainfall, which will then help to clarify the mechanism of the collapse in the nature.

[6]The strong internal variability also implies a substantial change of the timing of the vegetation collapse in different realizations. In another similar transient simulation that exhibits a vegetation collapse, we performed a 3-member 300-year ensemble simulations, which are initialized at different times about 100 years before the vegetation collapse. The collapse timings vary dramatically in these runs, with most of the runs showing no clear signal of collapse in the 300 years.

Acknowledgments

The authors would like to thank Drs. M. Claussen, P. Hoelzmann and an anonymous reviewer for helpful

comments. This work is supported by ESH/NSF. The computation is performed at NCAR CSL.

Appendix A. Regional analysis of model and data consistency over Northern Africa

Holocene paleovegetation and paleohydrological data over northern Africa mainly derive from lake, swamp and pollen records, and to a lesser extent, from vegetal and faunal macrorests, groundwater studies, eolian deposits, and archeological archives. In the context of our model simulation, we present a brief overview of regional differences in the climate-ecosystem evolutions and some examples illustrating increased hydro-climatic variability during the Late Holocene.

An examination of individual terrestrial records (see sites in Fig. 7) can reveal some differences in the regional paleoclimatic patterns, provided the local hydrological and vegetational dynamics, and the response time of individual systems and proxies to climate changes are considered. However, it is important to point out that any model/data comparison should be treated with caution, especially on the regional scale, because of the deficiencies in both the model and proxy records. Our model has a coarse resolution and a wet bias. Regional features tend to be less robust than those at large scales. Furthermore, implications of the proxy evidence also need to be kept in mind. The exact timing and rate of the Holocene decrease in water availability is often difficult to establish because: (i) a large number of records is truncated by wind deflation; (ii) many records suffer chronological uncertainties and have low time resolution; (iii) many water bodies were supplied by near-surface aquifers; the presence/absence of lakes and swamps (and hence pollen grains entrapped in their sediments) reflect a threshold response to the water table fluctuations, the rate of which cannot be estimated when the water table extent below the bottom of the topographic depressions and the lakes were dry. A time-transgressive fading can be related to the ecosystem's buffer capacity; (iv) vegetation also depends on the local water availability and of its threshold effects. Dominant vegetation types are generally derived from percentages of pollen taxa, but little information of pollen fluxes often limits the knowledge on density of the vegetation coverage. Nevertheless, selected sites provide relevant information on the aridification steps. Besides the chronology reliability, selection criteria are: (i) multi-proxy analysis because no indicator is unequivocal; (ii) several records from a same region for discarding the effects of individual systems' specificities; (iii) systems having a short-time response to climate changes. Area 1 coincides with the driest part of the present-day Sahara. Good representative sites lie in NW Sudan, East of 23°E, where several records (e.g., S1–S3, Fig. 7) document a consistent wet phase between ~10.5 and 6.4 ka followed by a single shift to dry conditions. For example, at Oyo (S2, Fig. 12b), lake sediment and pollen studies show that (Ritchie et al, 1985; Ritchie, 1994): (i) from ~9.5 to ~7 ka, the site supported a permanent lake surrounded by a continuous deciduous savanna vegetation under a humid tropical climate with annual monsoonal rainfall $\geqslant$400 mm,; (ii) a reduction in precipitation or in P–E initiated a shallowing of the lake from ~6.9 ka and a rapid southward retreat of the tropical savanna; annual precipitation declined from 300 mm at 6.9 ka to $<$100 mm at 5.4 ka when a Sahelian–Saharan vegetation predominated; the appearance of Saharan–Mediterranean pollen taxa suggests increasing interaction with northern, Atlantic/Mediterranean cyclonic systems; at 5.4 ka, the lake basin dried out and was covered subsequently by eolian and sebkhas sediments, whereas the vegetation, in the form of desert scrub-grasslands, disappeared except at oases and wades. These observations broadly agree with results from Fig. 4 and with the marine dust record at Site 658. However, the climatic deterioration initiated much earlier than 5.5 ka, and the basin desiccation started earlier in the north (S1: 6.5–5.2 ka) and later in the south (S3: 4.5–4.2 ka; in Hoelzmann et al., 2004).

Very little information is available for area 2, which extends north of the Tropics. Some Early-Mid Holocene lacustrine and sebkka deposits, paleosols and active river channels were found in southern Algeria. Paleolakes from the northern margin of the Sahara shifted from fresh- to hypersaline waterbodies in a few centuries at the Mid–Late Holocene transition, e.g., from 5 to 4.5 ka at site S9 (Fig. 12a; Gasse, 2002), but these sites were likely outside of the monsoon domain. From the coupled analysis of geological data and mesoscale climate modeling for northern Mali, the simulated paleoprocipitation showed a strong negative gradient north of 16–18°N and Early Holocene precipitation reaches a minimum value of 150–240 mm yr^{-1} at 22–24°N (Street-Perrott et al., 1990). Therefore, most of area 2 likely had a sparse, desert or semi-desert vegetation, although Hoelzmann et al. (1998) have suggested that the steppe–savanna boundary have reached 24–25°N in southern Algeria.

As area 1, area 3 was crossed by the savanna–desert boundary during the Early Holocene. Charcoal and pollen analysis indicate the presence of Sudanian savanna elements in the Ténéré desert at ca 19°N (e.g., S4, S5), suggesting higher annual precipitation of at least 350 mm (in Hoelzmann et al., 2004) than the ~10 mm today. Most lake records document two major Early-Mid Holocene phases of lake highstand induced by local rainfall and water table rises, or surface runoff. They are dated between ~11–8.5 and ~7.5–6.3 ka in northern Niger, 19–21°N (e.g., S6–S7) and between ~10.8–7.8 and ~6.3–5.1 ka in northern Mali, 20–23°N (S10–S12). Later on, a return to slightly moister conditions have been identified at a few sites, e.g., around 4 ka at site S6. These data are roughly consistent with the dust record off Mauritania. Nevertheless, the time of the major climate deterioration leading to modern conditions in area 3 decreases from North to South, as in area 1. Interestingly, the scenario suggested for area 3 (Fig. 6) would better represent the environmental evolution

recorded south of 18°N. In the present day-Sahel belt (~13–16°N; precipitation: 250–600 mm yr^{-1}), the establishment of modern conditions, although starting as soon as 8–6.0 ka, appears to have been more gradual and delayed compared to the Sahara desertification. This is possibly due to the lower sensitivity of this wetter region to the precipitation thresholds, which have generated both vegetation and lake collapse in the Sahara. Several sites (e.g., S13–S15) show a complex, step-wise, aridification trend, which started earlier and ended much later than 5.5 ka. For example, at site S14 (Fig. 12c), a step-wise decrease in tropical trees from 6.8 to 3.4 ka (Salzmann and Waller, 1998) is in phase with a decline of the lake water balance reflected in the diatom-inferred water conductivity (Gasse, 2002) and $\delta^{18}O$ records (Holmes et al., 1998, 1999). A return to wetter conditions at 4.5–4.0 ka occurred at sites S13 (Fig. 1d), S14 and S15, apparently in phase with that observed in Ethiopian lakes (S18, Fig. 1e, S17, Fig. 12d), then the aridification trend accelerated. At site S16, the palynological and palaeolimnological data demonstrate that the humid period terminated after ca 7.8 ka in a gradual decline of the precipitation/evaporation ratio and was not interrupted by abrupt climatic events. The aridification trend intensified after 4.2 ka and continued until the present (Salzmann et al., 2002). Apparently, the model overestimates precipitation and vegetal cover in areas 2 and 3. Better data-model agreement would occur if the model areas 2 and 3 would be shifted by 4–5° southward.

Increased climate variability after the wet Early–Mid Holocene period is documented by some records from northern Africa, in agreement with the model. At site S9 (Fig. 12a), the huge range of $\delta^{18}O$-values of biogenic carbonates from 5 to 4.5 ka indicates a large hydroclimatic unstability on the interannual scale. At site S14 (Fig. 12c), the Late Holocene period has been punctuated by several major droughts. Both the $\delta^{18}O_{ostracode}$ and the diatom-inferred salinity records (Gasse, 2002) document several major droughts and short periods more arid than today, e.g., between 2 and 1 ka. At Lake Tilo (S17, Fig. 12d), the $\delta^{18}O$ profile shows hydrological fluctuations of very high frequency after 4 ka, following a gradual shift in the hydrological balance from ca 8–4 ka (Lamb et al., 2000).

References

Abell, P.I., Hoelzmann, P., 2000. Holocene paleoclimates in northwestern Sudan: stable isotopes studies on mollusks. Global and Planetary Change 26, 1–12.

Adkins, J., deMenocal, P., Eshel, G., 2006. The "African Humid Period" and the record of marine upwelling from excess ^{230}Th in ODP hole 658C. Paleoceanography 21, PA4203.

Bard, E., Rostek, F., Turon, J., Gendreau, S., 2000. Hydrological impact of Heinrich events in the subtropical Northeast Atlantic. Science 289, 1321–1323.

Berger, A., 1978. Long-term variation of daily insolation and Quaternary climatic changes. Journal of Atmospheric Science 35, 2362–2367.

Berger, A., Loutre, M.-F., 1991. Insolation values for the climate of the last 10 million years. Quaternary Science Reviews 10, 297–317.

Brovkin, V., Claussen, M., Petoukhov, V., Ganopolski, A., 1998. On the stability of the atmosphere-vegetation system in the Sahara/Sahel region. Journal of Geophysical Research 103 (D24), 31613–31624.

Brovkin, V., Bendtsen, J., Claussen, M., Ganopolski, A., Kubatzki, C., Petoukhov, V., Andreev, A., 2002. Carbon cycle, vegetation and climate dynamics in the Holocene: experiments with the CLIMBER-2 Model. Global Biogeochemical Cycles 16 (4), 1139.

Chalié, F., Gasse, F., 2002. Late Glacial-Holocene diatom record of water chemistry and lake level change from the tropical East African Rift Lake Abiyata (Ethiopia). Palaeogeography, Palaeoclimatology, Palaeoecology 187, 259–283.

Charney, J.G., 1975. Dynamics of deserts and drought in the Sahel. Quarterly Journal of the Royal Meteorological Society 101, 193–202.

Claussen, M., 1994. On coupling global biome models with climate models. Climate Research 4, 203–221.

Claussen, M., 1997. Modeling biogeophysical feedback in the African and Indian Monsoon region. Climate Dynamics 13, 247–257.

Claussen, M., 1998. On multiple solutions of the atmosphere–vegetation system in present-day climate. Global Change Biology 4, 549–559.

Claussen, M., Gayler, V., 1997. The greening of Sahara during the Mid-Holocene: results of an interactive atmosphere–biome model. Global Ecology and Biogeography Letters 6, 369–377.

Claussen, M., Brovkin, V., Ganopolski, A., Kubatzki, C., Petoukhov, V., 1998. Modelling global terrestrial vegetation—climate interaction. Philosophical Transactions of the Royal Society of London Series B 353, 53–63.

Claussen, M., Kubatzki, C., Brovkin, V., Ganopolski, A., Hoelzmann, P., Pachur, H.-J., 1999. Simulation of an abrupt change in Saharan vegetation in the Mid-Holocene. Geophysical Research Letters 26, 2037–2040.

deMenocal, P., Ortiz, J., Guilderson, T., Adkins, J., Sarnthein, M., Baker, L., Yarusinksy, M., 2000. Abrupt onset and termination of the African Humid Period: rapid climate responses to gradual insolation forcing. Quaternary Science Reviews 19, 347–361.

Drake, J., Foster, I., Michalakes, J., Toonen, B., Worley, P., 1995. Design and performance of a scalable parallel community climate model. Parallel Computing 21, 1571–1591.

Finney, B.P., Johnson, T.C., 1991. Sedimentation in Lake Malawi (East Africa) during the past 10,000 years: a continuous paleoclimate record from the southern tropics. Palaeogeography, Palaeoclimatology, Palaeoecology 85, 351–366.

Fleitmann, D., Burns, S.J., Mudelsee, M., Neff, U., Kramers, J., Mangini, A., Matter, A., 2003. Holocene forcing of the Indian monsoon recorded in a stalagmite from Southern Oman. Science 300, 1737–1739.

Gallimore, R., Jacob, R., Kutzbach, J., 2005. Coupled atmosphere–ocean–vegetation simulations for modern and Mid-Holocene climates: role of extratropical vegetation cover feedbacks. Climate Dynamics.

Gasse, F., 2000. Hydrological changes in the African tropics since the Last Glacial Maximum. Quaternary Science Reviews 19, 189–211.

Gasse, F., 2002. Diatom-inferred salinity and carbonate oxygen isotopes in Holocene water bodies of the western Sahara and Sahel (Africa). Quaternary Science Reviews 21, 737–767.

Gasse, F., Roberts, N., 2004. Late Quaternary hydrologic changes in the arid and semi-arid belt of northern Africa. Implications for past atmospheric circulation. In: Diaz, H.F., Bradley, R.S. (Eds.), The Hadley Circulation: Present, Past and Future. Kluwer Ac. Pub., Dordrecht, pp. 313–345.

Gasse, F., Van Campo, E., 1994. Abrupt post-glacial climate events in West Asia and North Africa monsoon domains. Earth and Planetary Science Letters 126, 435–456.

Gasse, F., Téhet, R., Durand, A., Gibert, E., Fontes, J.C., 1990. The arid-humid transition in the Sahara and Sahel during the last deglaciation. Nature 346, 141–146.

Hack, J.J., Bouville, B.A., Brieglib, B.P., Kiehl, J.T., Rasch, P.J., Williamson, D.L., 1993. Description of the NCAR Community Climate Model (CCM2). NCAR Technical Note NCAR/TN-382+STR, Boulder, CO, 108p.

Halfman, J.D., Jacobson, D.F., Cannella, C.M., Haberyan, K.A., Finney, B.P., 1992. Fossil diatoms and the Mid to Late Holocene paleolimnology of Lake Turkana, Kenya: a reconaissance study. Journal of Paleolimnology 7, 23–35.

Haxeltine, A., Prentice, I.C., 1996. BIOME3: an equilibrium terrestrial biosphere model based on ecophysiological constraints, resource availability, and competition among plant functional types. Global Biogeochemical Cycles 10, 693–709.

Hewitt, C.D., Mitchell, J.F.B., 1998. A fully coupled GCM simulation of the climate of the Mid-Holocene. Geophysical Research Letters 25, 361–364.

Hoelzmann, P., Gasse, F., Dupont, L.M., Salzmann, U., Staubwasser, M., Leuchner, D.C., Sirocko, F., 2004. Palaeoenvironmental changes in the arid and subarid belt (Sahara–Sahel–Arabian Peninsula) from 150 ka to present. In: Battarbee, R.W., Gasse, F., Stickley, C.S. (Eds.), Past Climate through Europe and Africa. Springer, Dordrecht, pp. 219–256.

Hoelzmann, P., Jolly, D., Harrison, S.P., Laarif, F., Bonnefille, R., Pachur, H.-J., 1998. Mid-Holocene land-surface conditions in northern Africa and the Arabian peninsula: a data set for the analysis of biogeophysical feedbacks in the climate system. Global Biochemical Cycles 12, 35–51.

Holmes, J.A., Fothergill, P.A., Street-Perrott, F.A., Perrott, R.A., 1998. A high-resolution Holocene record from the Sahel Zone of northeastern Nigeria. Journal of Paleolimnology 20, 369–380.

Holmes, J.A., Street-Perrott, F.A., Perrott, R.A., Stokes, S., Waller, M.P., Huang, Y., Eglington, G., Ivanocich, M., 1999. Holocene landscape evolution of the Manga grasslands, NE Nigeria: evidence from palaeolimnology and dune chronology. Journal of Geological Society, London 156, 357–358.

Jacob, R.L., 1997. Low frequency variability in a simulated atmosphere ocean system. Ph.D. Thesis, University of Wisconsin, Madison.

Jolly, D., et al., 1998. Biome reconstruction from pollen and plant cacrofossil data for Africa and the Afabian peninsula at 0 and 6000 years. Journal of Biogeography 25, 1007–1028.

Johnson, T.C., Kelts, K., Odada, E.O., 2000. The Holocene history of Lake Victoria. AMBIO 29, 2–11.

Jung, S.J.A., Davies, G.R., Ganssen, G.M., Kroon, D., 2004. Stepwise Holocene aridification in NE Africa deduced from dust-borne radiogenic isotope records. Earth and Planetary Science Letters 221, 27–37.

Kitoh, A., Yamazai, K., Tokioka, T., 1988. Influence of soil moisture and surface albedo changes over the African tropical rainforest on summer climate investigated with the MRI-GCM-I. Journal of the Meteorological Society of Japan 66, 65–85.

Kubatzki, C., Claussen, M., 1998. Simulation of the global biogeophysical interactions during the last glacial maximum. Climate Dynamics 14, 461–471.

Kuper, R., Kropelin, S., 2006. Climate-controlled Holocene occupation in the Sahara: motor of Africa's evolution. Science 313, 803–807.

Kutzbach, J.E., Liu, Z., 1997. Response of the African monsoon to orbital forcing and ocean feedbacks in the Middle Holocene. Science 278, 440–444.

Kutzbach, J.E., Otto-Bliesner, B.L., 1982. The sensitivity of the African–Asian monsoonal climate to orbital parameter changes for 9000 years BP in a low-resolution geneal circulation model. Journal of Atmospheric Science 39, 1177–1188.

Kutzbach, J.E., Street-Perrott, F.A., 1985. Milankovitch forcing of fluctuations in the level of tropical lakes from 18 to 0 ka. Nature 317, 130–134.

Kutzbach, J.E., Bonan, G., Folly, J., Harrison, S.P., 1996. Vegetation and soil feedbacks on the response of the African monsoon to orbital forcing in the Early to Middle Holocene. Nature 384, 623–626.

Lamb, A.L., Leng, M.J., Lamb, H.F., Mohammed, M.U., 2000. A 9000-year oxygen and carbon isotope record of hydrological change in a small Ethiopian crater lake. The Holocene 10, 167–177.

Lézine, A.M., 1989. Late Quaternary vegetation and climate of the Sahel. Quaternary Research 32, 314–334.

Lézine, A.-M., Casanova, J., 1989. Pollen and hydrological evidence for the interpretation of past climates in tropical West Africa during the Holocene. Quaternary Science Reviews 8, 45–55.

Liu, Z., Yang, H., 2003. Extratropical control on tropical climate: atmospheric bridge and oceanic tunnel. Geophysical Research Letters 30.

Liu, Z., Gallimore, R., Kutzbach, J., Xu, W., Golubev, Y., Behling, P., Siegle, R., 1999. Modeling long term climate change with the Equilibrium Asynchronous Coupling scheme. Climate Dynamics 15, 325–340.

Liu, Z., Kutzbach, J., Wu, L., 2000. Modeling climate shift of El Niño in the Holocene. Geophysical Research Letters 27, 2265–2268.

Liu, Z., Otto-Bliesner, B., Kutzbach, J., Li, L., Shields, C., 2003a. Coupled climate simulation of the evolution of global monsoons in the Holocene. Journal of Climate 16, 2472–2490.

Liu, Z., Brady, E., Lynch-Steiglitz, J., 2003b. Global ocean response to orbital forcing in the Holocene. Paleoceanography 18 (2), 1041.

Liu, Z., Zhang, Q., Wu, L., 2004. The remote impact on tropical Atlantic climate variability: the dynamic assessment and statistical assessment. Journal of Climate 17, 1529–1549.

Liu, Z., Wang, Y., Gallimore, R., Notaro, M., Prentice, C.I., 2006a. On the mechanism of abrupt change of Northern Africa environment in the Holocene: climate variability vs. vegetation feedback. Geophysical Research Letters 33, L22709.

Liu, Z., Notaro, M., Kutzbach, J., Liu, N., 2006b. Assessing global vegetation-climate feedbacks from the observation. Journal of Climate 19 (5), 787–814.

Müller, P.J., Fischer, G., 2001. A 4-year sediment trap record of alkenones from the filamentous upwelling region off Cape Blanc, NW Africa and a comparison with distributions in underlying sediments. Deep-Sea Research I 48, 1877–1903.

Notaro, M., Liu, Z., Gallimore, R., Vavrus, S.J., Kutzbach, J.E., Prentice, I.C., Jacob, R.L., 2005. Simulated and observed pre-industrial to modern vegetation and climate changes. Journal of Climate 18, 3650–3671.

Notaro, M., Wang, Y., Liu, Z., Gallimore, R., Levis, S., 2007. Combined statistical and dynamical assessment of the simulated negative vegetation feedback on North African annual precipitation during the Mid-Holocene. Global Change Biology, submitted.

Pailler, D., Bard, E., 2002. High frequency palaeoceanographic changes during the past 140,000 yr recorded by the organic matter in sediments of the Iberian Margin. Paleoceanography, Paleoclimatology, Palaeoecology 181, 431–452.

Renssen, H., Brovkin, V., Fichefet, T., Goosse, H., 2003. Holocene climate instability during the termination of the African Humid Period. Geophysical Research Letters 30, 1184.

Ritchie, J.C., 1994. Holocene pollen spectra from Oyo, northwestern Sudan: problems of interpretation in an hyperarid environment. The Holocene 4 (1), 9–15.

Ritchie, J.C., Haynes, C.V., 1987. Holocene vegetation zonation in the eastern Sahara. Nature 330, 645–647.

Ritchie, J.C., Eyles, C.H., Haynes, C.V., 1985. Sediment and pollen evidence for an Early to Mid-Holocene humid period in the eastern Sahara. Nature 314, 352–355.

Russell, J.M., Johnson, T.C., Kelts, K.R., Laerdal, T., Talbot, M.R., 2003. An 11,000-year lithostratigraphic and paleohydrologic record from equatorial Africa: Lake Edward, Uganda-Congo. Palaeogeography, Palaeoclimatology, Palaeocecology 193, 25–49.

Salzmann, U., Waller, M., 1998. The Holocene vegetational history of the Nigerian Sahel based on multiple pollen profiles. Review of Palaeobotany and Palynology 100, 39–72.

Salzmann, U., Hoelzmann, P., Morcinek, I., 2002. Late Quaternary climate and vegetation of the Sudanian zone of NE Nigeria. Quaternary Research 58, 73–83.

Sankaran, M., Hanan, N., et al., 2005. Determinants of woody cover in African savannas. Nature 438, 846–849.

Schurgers, G., Mikolajewicz, U., Gröger, M., Maier-Reimer, E., Vizcaíno, M., Winguth, A., 2006. Changes in terrestrial carbon storage during

interglacials: a comparison between Eemian and Holocene. Climate of the Past, in press.

Shukla, J., Mintz, Y., 1982. Influence of land-surface evapotranspiration on earth's climate. Science 215, 1498–1501.

Sitch, S., 2000. The role of vegetation dynamics in the control of atmospheric CO_2 content. Ph.D. Dissertation, Lund University, Lund, 213p.

Sitch, S., Smith, B., Prentice, I.C., Arneth, A., Bondeau, A., Cramer, W., Kaplan, J.O., Levis, S., Lucht, W., Sykes, M.T., Thonicke, K., Venevsky, S., 2003. Evaluation of ecosystem dynamics, plant geography and terrestrial carbon cycling in the LPJ dynamic global vegetation model. Global Change Biology 9, 161–185.

Street-Perrott, F.A., Mitchell, J.F.B., Marchand, D.S., Brunner, J.S., 1990. Milankovitch and albedo forcing of the tropical monsoons: a comparison of geological evidence and numerical simulations for 9000 yr BP. Transactions of the Royal Society of Edinburgh: Earth Sciences 81, 407–427.

Wang, G., Eltahir, E.A.B., 2000. Biosphere–atmosphere interactions over West Africa 2. Multiple equilibria. Quarterly Journal of the Royal Meteorological Society 126, 1261–1280.

Wang, W.L., Anderson, B.T., Phillips, N., Kaufmann, R.K., Potter, C., Myneni, R.B., 2006. Feedbacks of vegetation on summertime climate variability over the North American grasslands: 1. Statistical analysis. Earth Interactions 10, 1–27.

Wang, Y., Mysak, L.A., Wang, Z., Brovkin, V., 2005. The greening of the McGill Paleoclimate Model: Part II. Simulation of Holocene millennial-scale natural climate changes. Climate Dynamics 24, 481–496.

Wang, Y., Notaro, M., Liu, Z., Gallimore, R., Levis, S., Kutzbach, J., 2007. Detecting vegetation-precipitation feedbacks in Mid-Holocene North Africa from two climate models. Geophysical Research Letters, submitted.

Wu, L., Liu, Z., 2005. North Atlantic decadal variability: air–sea coupling, oceanic memory, and potential Northern Hemisphere resonance. Journal of Climate 18, 331–349.

Wu, L., Liu, Z., Gallimore, R., 2003. Pacific decadal variability: the tropical Pacific mode and North Pacific mode. Journal of Climate 16, 1101–1120.

Xue, Y., Shukla, J., 1993. The influence of land surface properties on Sahel climate: part I: Desertification. Journal of Climate 6, 2232–2245.

Zhao, M., Beveridge, N.A.S., Shackleton, N.J., Sanrthein, M., Eglinton, G., 1995. Molecular stratigraphy of cores off northwest Africa: sea surface temperature history over the last 80 ka. Paleoceanography 10, 661–675.

Zhao, M., Dupont, L., Eglinton, G., Teece, M., 2003. *n*-alkane and pollen reconstruction of terrestrial climate and vegetation for NW Africa over the last 160 kyr. Organic Geochemistry 34, 131–143.

Zeng, N., Neelin, J.D., 2000. The role of vegetation-climate interaction and interannual variability in shaping the African savanna. Journal of Climate 13, 2665–2670.